



저작자표시-비영리-변경금지 2.0 대한민국

이용자는 아래의 조건을 따르는 경우에 한하여 자유롭게

- 이 저작물을 복제, 배포, 전송, 전시, 공연 및 방송할 수 있습니다.

다음과 같은 조건을 따라야 합니다:



저작자표시. 귀하는 원저작자를 표시하여야 합니다.



비영리. 귀하는 이 저작물을 영리 목적으로 이용할 수 없습니다.



변경금지. 귀하는 이 저작물을 개작, 변형 또는 가공할 수 없습니다.

- 귀하는, 이 저작물의 재이용이나 배포의 경우, 이 저작물에 적용된 이용허락조건을 명확하게 나타내어야 합니다.
- 저작권자로부터 별도의 허가를 받으면 이러한 조건들은 적용되지 않습니다.

저작권법에 따른 이용자의 권리는 위의 내용에 의하여 영향을 받지 않습니다.

이것은 [이용허락규약\(Legal Code\)](#)을 이해하기 쉽게 요약한 것입니다.

[Disclaimer](#)

Master's Thesis

Numerical and Experimental Analysis of
the Drilling Process of the CFRP-Metal Stack

Yeonoh Kim

Department of Mechanical Engineering

Graduate school of UNIST

2019

Master's Thesis

Numerical and Experimental Analysis of the
Drilling Process of the CFRP-Metal Stack

Yeonoh Kim

Department of Mechanical Engineering

Graduate School of UNIST

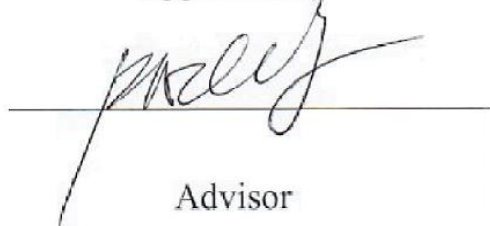
Numerical and Experimental Analysis of the Drilling Process of the CFRP-Metal Stack

A thesis
submitted to the Graduate School of UNIST
in partial fulfillment of the
requirements for the degree of
Master of Science

Yeonoh Kim

11. 28. 2018

Approved by

A handwritten signature in black ink, appearing to read 'HWPark', is written over a horizontal line. The signature is fluid and cursive.

Advisor

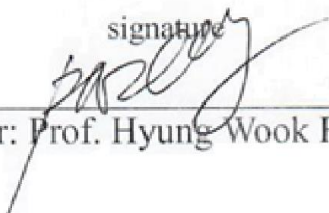
Prof. Hyung Wook Park


Numerical and Experimental Analysis of the Drilling Process of the CFRP-Metal Stack

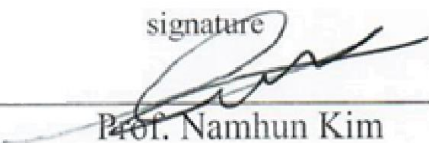
Yeonoh Kim

This certifies that the thesis of Yeonoh Kim is approved.

11. 28. 2018 of submission

signature

Thesis Supervisor: Prof. Hyung Wook Park

signature

Prof. Young-Bin Park

signature

Prof. Namhun Kim

ABSTRACT

In the present study, researchers are more focused on aerospace and automotive fields, however, in this field very difficult task to reduce the inertia of the bodies through a lightweight material with high strength. To reduce this problem, researchers are focused on the CFRP due to its lightweight and its high strength. Carbon fiber reinforced plastic (CFRP) is superior in weight to strength ratio as compared to metal. It is moreover excellent in abrasion resistance and heat resistance. For this reason, CFRP is being used as a functional component material in the transportation industry and automobile industry. Despite the many advantages of CFRP, CFRP is vulnerable to impact and brittle than metal. The main issues during composite materials processing are delamination. The delamination significantly reduces assembly tolerance and strength against fatigue, which reduces the long-term performance of the composite. The size of the delamination zone is related to the thrust force generated in the drilling process, a critical thrust force is generated which does not cause damage. Therefore, several studies have investigated delamination during the drilling process.

In this study, numerical models are used to predict thrust force and internal defects in the CFRP-Al stacks drilling process. The physical model is used to generate the mechanism of the thrust force by using the chisel edge and a lip region of the tool, to create a prediction model. The thrust force in the CFRP-Al stack was predicted by the thrust force measured at each part of the tool. FE model (ABAQUS/ Explicit) is used for the prediction of thrust force in the delamination drilling simulation. In the delamination of the material, seven layers of CFRP and one layer of aluminum is used to identify the internal defects in each layer. To represent the multi-direction CFRP, CFRP consisting of 7 layers was modelled at 0° and 90° . In this simulation process two damage model are used for defining the material property of the materials. First one is the Hashin's damage model, used for defining the property of the CFRP material. The second one is the Johnson-cook model, used for defining the property of the aluminum because it represents the internal defects and CFRP-Al stack expressed through cohesive conditions. Moreover, stress contour has been confirmed during CFRP-Al stack drilling simulation. To validate the numerical model, thrust force and machinability were investigated by CFRP-Al stack drilling process and in this process identified the internal defect which is compared by CT scan. Based on the developed prediction model, it is considered that the optimal machining conditions have been derived in the CFRP-Al stack drilling process.

CONTENTS

1. INTRODUCTION	1
1.1 Background	1
1.2 Research objectives and approach	2
1.3 Dissertation organization	4
2. LITERATURE REVIEW	5
2.1 Theory of Carbon Fiber Reinforced Plastic (CFRP) cutting	5
2.2 Mechanism of the Drilling Process.....	8
2.3 Numerical Studies on Drilling	8
2.3.1 Modelling of CFRP	9
2.3.2 Modelling of Metal.....	11
2.3.3 Modelling of the CFRP-Metal stack.....	13
2.4 Summary.....	15
3. PHYSICAL MODEL OF DRILLING IN CFRP-METAL STACK.....	16
3.1 Modelling of the drilling process	16
3.1.1 Force formulation in the chisel edge.....	17
3.1.2 Force formulation in the cutting lip region	19
3.2 Material property	24
3.3 Summary	25
4. FINITE ELEMENT MODEL OF DRILLING IN CFRP-METAL STACK	26
4.1 FE model setup.....	26
4.1.1 Geometry modelling and boundary conditions	27
4.1.2 Finite elements and mesh type	28
4.2 Material property	29
4.2.1 Aluminum modelling	30
4.2.2 CFRP damage modelling	33
4.3 Delamination modelling	36
4.4 Summary	38

5. ANALYSIS OF PHYSICAL MODEL AND FINITE ELEMENT MODEL	39
5.1 Physical model analysis	39
5.2 FE model analysis	40
5.3 Comparison and analysis between the physical model and FE model.....	47
5.4 Summary	48
6. EXPERIMENTAL VALIDATION	49
6.1 Experimental setup.....	49
6.2 Experimental results.....	52
6.2.1 Thrust force	52
6.2.2 Delamination	53
6.3 Numerical model validation.....	56
6.3.1 Thrust force validation.....	56
6.3.2. Delamination validation	58
6.4 Summary	61
7. CONCLUSIONS AND FUTURE WORKS.....	62
7.1 Contributions and Conclusions.....	62
7.2 Future works.....	63
REFERENCES	64
ACKNOWLEDGEMENTS	70

LIST OF FIGURES

Fig. 1-1. Global demand for carbon fiber from 2010 to 2022.....	1
Fig. 1-2. Experimental process for numerical model optimization.....	3
Fig. 1-3. Flowchart of dissertation organization	4
Fig. 2-1. Orthogonal cutting model of composite	6
Fig. 2-2. Cutting mechanisms in orthogonal cutting.....	7
Fig. 2-3. Cross-section on the cutting lip region.....	9
Fig. 2-4. Stresses contour in a workpiece for the case of 0.1mm depth.....	10
Fig. 2-5. Workpiece model.....	11
Fig. 2-6. Stress contour of FE model	12
Fig. 2-7. Thrust force and torque in drilling experiment. Diameter = 8 mm, 1050 rpm, feed = 0.10 mm/rev	13
Fig. 2-8 Fig. 2-8. Compare the critical thrust force results (a) drilling aluminum to CFRP (b) drilling CFRP to aluminum	14
Fig. 2-9. Thrust force and torque in CFRP-Al-CFRP stack drilling process	14
Fig. 2-10. The 3-dimentional model of the CFRP-Al stack	15
Fig. 3-1 Flowchart for the modelling process	16
Fig. 3-2. A complete cycle of the drilling process. Chisel edge engagement (Stage 1), lip region engagement (Stage 2), full engagement (Stage 3), interface region (Stage 4), full engagement (Stage 5), exit region (Stage 6).....	17
Fig. 3-3. The cutting effect of chisel edge.....	18
Fig. 3-4. The cutting effect of lip region.....	19
Fig. 3-5. Three regions of orthogonal cutting	20
Fig. 3-6. Schematic of CFRP orthogonal cutting in Region 2	21
Fig. 3-7. Force transformation for the drilling system	22
Fig. 3-8. Change in cutting radius over time.....	23
Fig. 4-1. Progress of CFRP-Al Stack drilling	26
Fig. 4-2. FE model geometry	27
Fig. 4-3. Boundary condition of the FE model	28
Fig. 4-4. Mesh of FE model (a) CFRP-Al stack, (b) Drill bit	29
Fig. 4-5. Strain-stress relationship of ductile material failure process.....	31
Fig. 4-6. Algorithm of VUMAT ABAQUS/Explicit.....	34
Fig. 4-7. Damage criterion and evolution in the interface cohesive	36

Fig. 5-1. Result of the physical model	39
Fig. 5-2. Critical thrust force in (a) CFRP part, (b) aluminum part	40
Fig. 5-3 Results of thrust force according to drill position	41
Fig. 5-4. Critical thrust force in (a) CFRP part, (b) aluminum part	42
Fig 5-5. CFRP-Al drilling simulation in FEM	43
Fig. 5-6. Stress contour of FE model	43
Fig. 5-7. Delamination in the FE model.....	44
Fig. 5-8 Measurement of delamination extent	46
Fig. 5-9. Comparison of the critical thrust force between the physical model and FE model	47
Fig. 6-1. Experimental set for CFRP-Al stack drilling	49
Fig. 6-2. Experimental conditions of CFRP-Al drilling process.....	50
Fig. 6-3. The CFRP-Al stack	50
Fig. 6-4. Design of the jig system (a) Top jig (b) Bottom jig.....	51
Fig. 6-5. CFRP-Al stack drilling experiment result	52
Fig. 6-6. Thrust force results according to each machining condition (a) CFRP part (b) aluminum part	53
Fig. 6-7. Delamination extent according to RPM in the same feed	54
Fig. 6-8. Delamination extent according to feed in the same RPM	54
Fig. 6-9. Experimental based delamination discrimination	55
Fig. 6-10. CFRP-Al stack internal defect (a) 1.42mm, (b) 0.91mm	55
Fig. 6-11. Comparison of Thrust Force between Simulation and Experimental Results (a) 6000rpm, 0.05mm/rev, (b) 6000rpm, 0.08mm/rev, (c) 6000rpm, 0.11mm/rev	57
Fig. 6-12. Comparison of critical thrust force results of two models and experiments	57
Fig. 6-13. Comparison of delamination between experimental and prediction model	60
Fig. 6-14. Variation of delamination	61

LIST OF TABLES

Table 3-1. Parameters of CFRP.....	24
Table 3-2. Parameters of Al.....	24
Table 4-1. Material properties of the simulated CFRP	30
Table 4-2. Material properties of the simulated Al6061	30
Table 4-3. Johnson-Cook material constants for Al 6061	31
Table 4-4. Johnson cook damage model parameters for Al6061	32
Table 4-5. Strength properties of Multi-direction CFRP	36
Table 4-6. Material properties used in cohesive of the interface	37

NOMENCLATURE

γ_f	the angle between the force of chisel edge and cutting direction
w	the half thickness of chisel edge
ψ	the rake angle of the chisel edge
γ_w	the half of the chisel edge angle
ε_d	the point angle
E	Young's modulus
ν	Poisson's ratio
f	feed rate
n	the rate of rotation
a_c	the cutting thickness
γ_{Al}	the shear stress
σ_{Al}	the yield stress
h	the width of a workpiece
β	the friction angle
γ_0	the rake angle of the cutting tool
θ_r	the helix angle of the drill bit
r_e	the tool nose radius
E^*	the effective elastic modulus
μ	the friction coefficient
α	the clearance angle
$i(\rho)$	the inclination angle
r_{chi}	the initial cutting length
ρ	the density
$\bar{\varepsilon}$	the effective plastic strain
$\dot{\bar{\varepsilon}}$	the effective plastic strain rate
$\dot{\bar{\varepsilon}}_0$	the normalizing strain rate
$\bar{\varepsilon}_i$	the equivalent plastic strain
ω	the scalar damage parameter
D	the failure parameters
P	the pressure
$\bar{\sigma}$	the Mises equivalent stress
$\Delta\bar{\varepsilon}$	the equivalent plastic strain increment

$\bar{\varepsilon}_i$	the equivalent plastic strain
$\bar{\varepsilon}_f$	the equivalent plastic failure
L	the length
σ_y	the yield stress
\bar{u}_f	the equivalent plastic displacement
t_n	the normal stress
t_t	the shear traction
G_n	the immediate fracture energies in normal direction
G_t	the immediate fracture energies in shear direction
G_n^c	the critical value
D_{ext}	the delamination extent

1. INTRODUCTION

1.1 Background

In today's aerospace and automotive fields, research and development of carbon dioxide regulation and light weight are becoming important [1]. Carbon fiber reinforced plastic (CFRP) is superior in denseness to density compared to metal and is excellent in abrasion resistance and heat resistance and does not rust [2-3]. In addition, there is strong demand for light-weighting for environmental regulation and fuel efficiency enhancement worldwide, so the technology development of processing companies is required. For this reason, CFRP is being used as a functional component material in the transportation industry. CFRP usage has been increasing rapidly, and this outlook will continue, as shown in fig. 1-1.

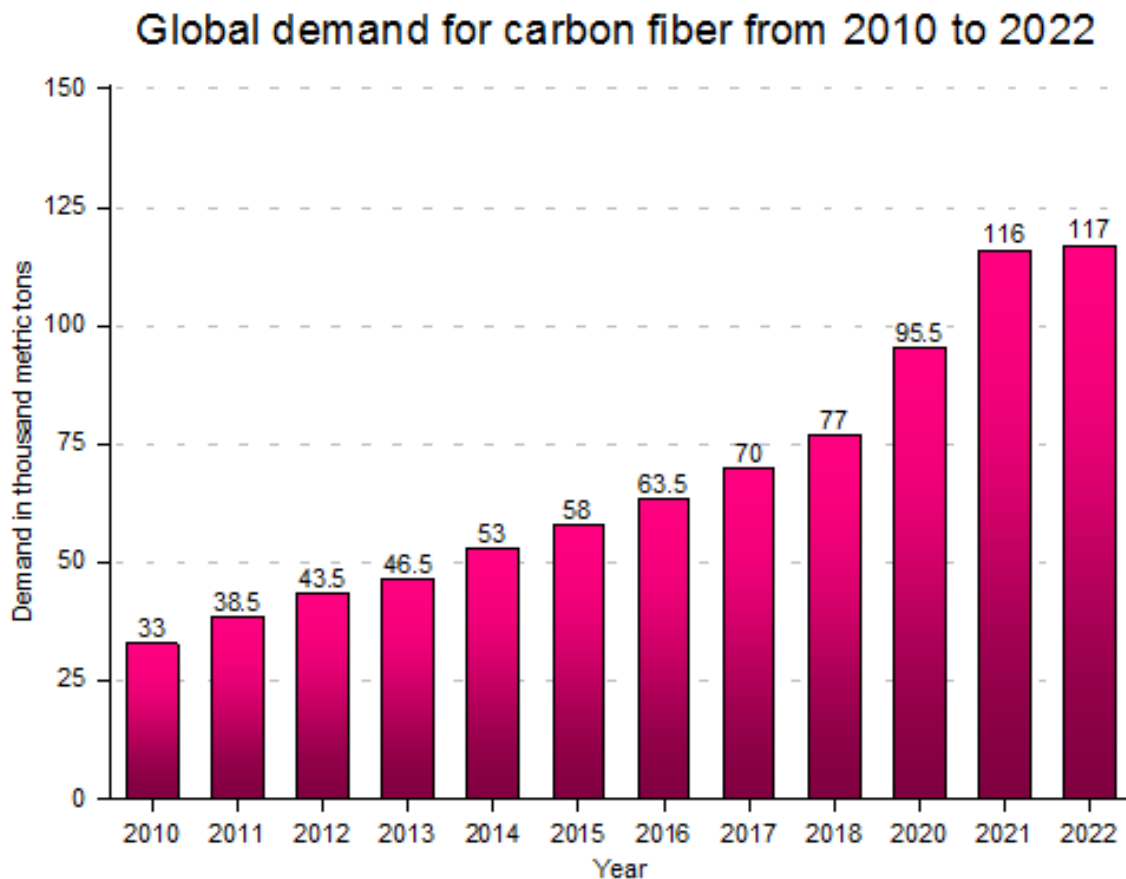


Fig. 1-1. Global demand for carbon fiber from 2010 to 2022 [4]

Despite the many advantages of CFRP, CFRP is vulnerable to impact and brittle than metal. To compensate for this, CFRP-metal stacks materials have been widely used in aerospace and automotive applications where a high load is applied [5]. All these materials are difficult to process, but technology development is required to compensate for the disadvantages of each material. The main issues during composite materials processing are delamination [6-7]. The delamination significantly reduces assembly tolerance and strength against fatigue, which reduces the long-term performance of the composite. The size of the delamination is related to the thrust force generated in the drilling process, and it is thought that there is a critical thrust force that does not cause damage. Therefore, several studies have investigated delamination during the drilling process [8-9]. In this study, a numerical model is used to predict thrust force and delamination in CFRP-Al composites drilling. The cutting condition and the boundary condition of each model were the same and the proper property was used for the model. There are three kinds of CFRP as Uni-direction (UD) CFRP, Multi-direction (MD) CFRP, and Fabric CFRP depending on methods of manufacturing. In this research, a combination of MD CFRP consisting of 0-degree / 90-degree layers of 3 mm thickness and Al 6061 of 2 mm thickness has been used. To validate the numerical model, thrust force and machinability were investigated by CFRP-Al stack drilling process. Furthermore, the developed FE model was available to predict defects and verified the model comparing the experimental results.

1.2 Research objectives and approach

Composite material characteristics are introduced previously. However, to solve defects occurring during machining, CFRP and metal-bonded stack materials are required. CFRP and metal stack materials have excellent mechanical properties. In addition, CFRP, which is vulnerable to shocks, can be supplemented. Although the CFRP-metal stack has these advantages, this material is also difficult to process. In the aerospace industry, riveting work is essential to combine materials, which requires drilling process. However, the drilling process is not easy due to the different machining properties of CFRP and metal materials. Internal defects occurs during the drilling process, which is related to critical thrust forces. Therefore, critical thrust force prediction is necessary to prevent internal defects.

This study suggests two kinds of the prediction model. The first prediction model is used with the Matlab software. In this model, thrust force was estimated by calculating the thrust forces at the chisel edge and lip region. Also, delamination discrimination was predicted based on an

experimental formula. The second one has been performed through the geometry simplification of the drill and CFRP-Al stacks to build the FE model using the commercial simulation tool by ABAQUS. In this model, the thrust force was predicted by setting a reference point at the drill point, and delamination was expressed using Hashin's criterion damage model and cohesive condition. The result of CFRP-Al stacks drilling numerical model is compared with the exactly similar setup of experimental results. In this numerical modelling and experiment, it can be helpful to identify the properties of CFRP-Al stacks drilling and increase the reliability of numerical models.

For this goal, this study includes four steps:

Step 1: Investigate the characteristics of CFRP drilling.

Step 2: Develop thrust force and delamination numerical prediction model.

Step 3: Experiment CFRP-Metal stack drilling for identifying the thrust force and defects.

Step 4: Verify the results of the numerical model compared to the experimental results.

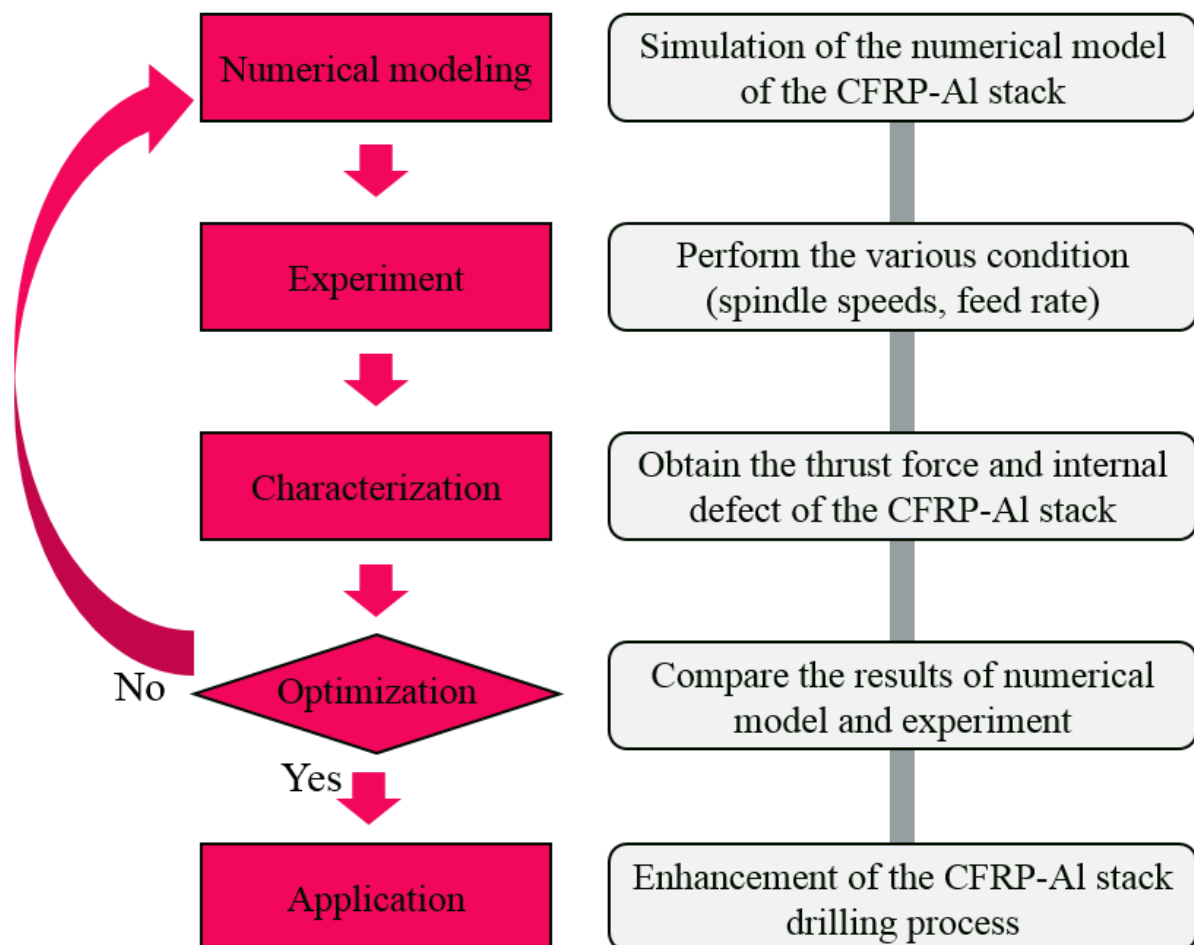


Fig. 1-2. Experimental process for numerical model optimization

1.3 Dissertation organization

Chapter-1 is based on the introduction part of this process. Chapter-2 shows the literature review. The literature review section shows studies in characteristics of CFRP and metal machining and numerical studies on the drilling process. Then, chapter-3 and chapter-4 describe the model of drilling in the CFRP-Metal stack. Chapter-3 is based on the physical model and FE model is described in chapter-4. In chapter-5, the models developed in chapter-3, 4 are analyzed and compared. Chapter-6 based on the comparison of results. In this chapter, the Physical model and FE model are compared with the experimental results regarding thrust force and defects. Finally, Chapter-6 describes the conclusions and future works. This dissertation is laid out as follows flowchart which is shown in fig. 1-3.

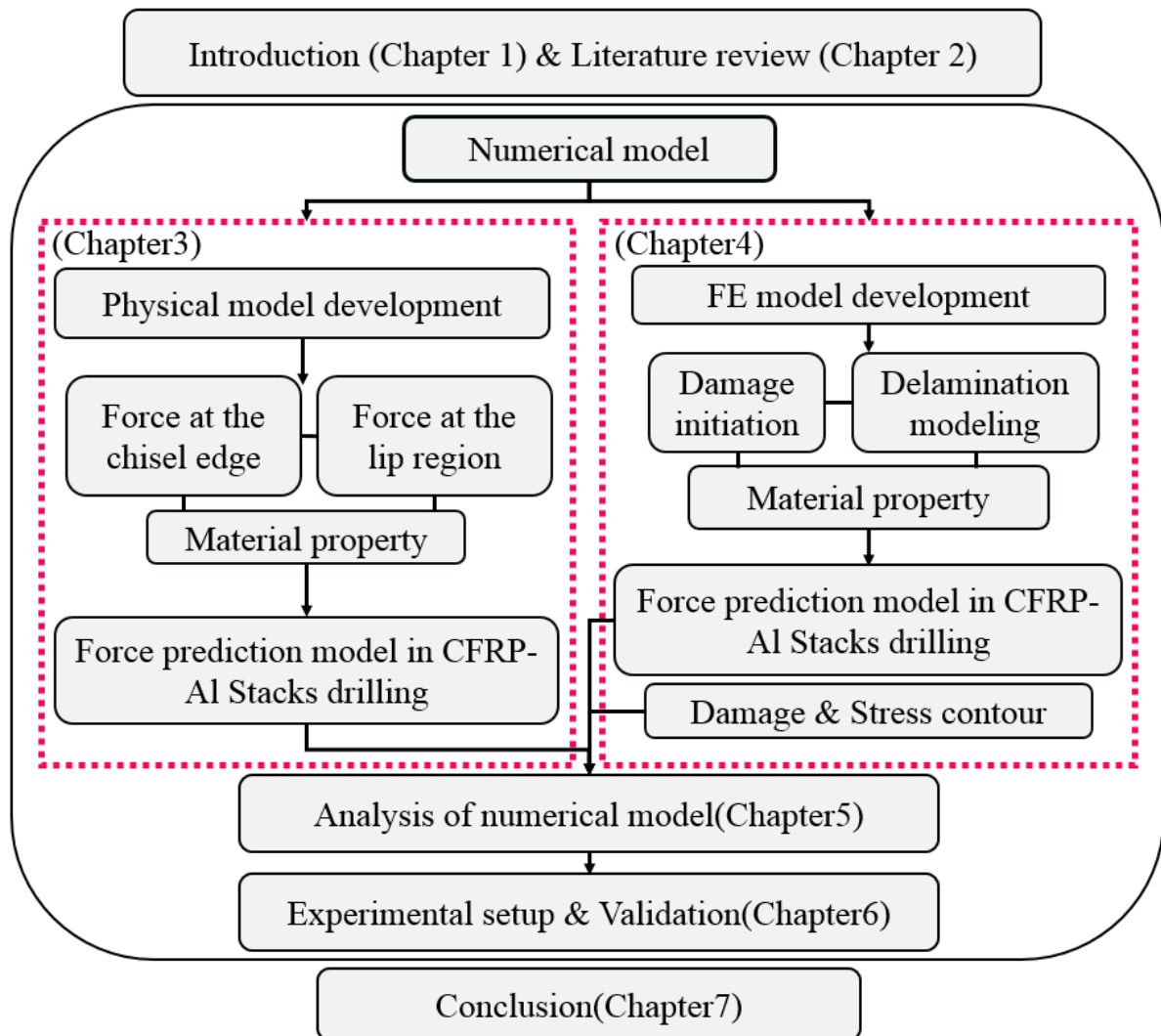


Fig. 1-3. Flowchart of dissertation organization.

2. LITERATURE REVIEW

This chapter is based on the review of the literature survey of these fields. This literature review includes three main components:

- (1) Theory of Carbon fiber reinforced plastic (CFRP) Cutting
- (2) Mechanics of the Drilling Process
- (3) Numerical studies on drilling

The literature review of the Numerical studies on drilling will include FEM process applied in the CFRP drilling system.

2.1 Theory of Carbon Fiber Reinforced Plastic (CFRP) Cutting

Research of the machining process for fiber reinforced plastics (FRP) has been going on for several years [10-12]. Researchers attempt to formulate new models for FRP composite machining based on existing tools and models, primarily of metal alloy processing. To develop a model for FRP composite materials machining process, it is necessary to understand the metal cutting mechanism and next, it is necessary to discuss the mechanism for the FRP composite material machining. Carbon fiber reinforced plastic (CFRP) has many advantages such as high strength based on density, abrasion resistance, heat resistance, and rust-free so today, CFRP is used in a variety of industries. However, CFRP is difficult to cut, unlike metals due to its brittleness in nature and non-homogeneity. It is difficult to predict cutting forces and surface conditions. The chip formation mechanism is defined by shearing in metallic alloys however, the chip formation is controlled by the bending in the fiber-matrix interface in the machining process of CFRP composite materials. The quality of machining surface is affected by its the fiber orientation. For these reasons, it is complicated to the machining of CFRP composite materials [13-15]. Therefore, the process of CFRP composite an appropriate mechanism considering fiber orientation and chip formation is required, and optimum processing conditions are required.

There have been many studies on FRP composites. According to the Koplev et al [16], the machining of CFRP is examined by experiments with chip preparation technique. Both two processing directions parallel and perpendicular to the fiber orientation of Unidirectional composite was performed

in a cutting operation. During unidirectional CFRP processing, parallel to the fibers, the horizontal cutting force is determined by the rake angle and the cutting depth. And the vertical cutting force is determined by the wear of the tool and the relief angle. The FRP has machinability depending on the mechanical properties of the composite and fiber orientation [17]. The carbon fibers tend to break into brittle form by the cutting edge, but the fibers tend to break off the fiber shear by bending at the cutting edge. Therefore, the surface quality depends on the fiber strength, orientation and it's cutting conditions are dependent on the fiber matrix strength. The chip formation is important for understanding the cutting mechanism of the FRP [18-20]. The polymer matrix in the FRPs is an important affectation in the chip formation and its types, since its strength and stiffness are low-grade than those of reinforcement fibers, and they have at least resistance as the cutting. H. Takeyama *et al.* [21] proposed the chip formation theory in the orthogonal cutting model of FRP. The chip formation of FRP is strongly influenced by the fiber orientation in relation to the cutting direction.

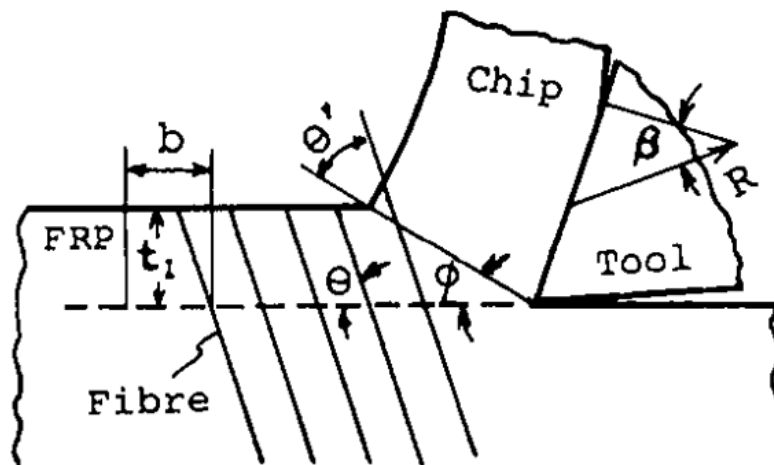


Fig. 2-1. Orthogonal cutting model of composite [21]

Where ϕ : Shear angle, θ : Fiber angle and θ' : Shear fiber angle

Wang *et al.* [22] suggested the cutting mechanism by diverse fiber orientation in composite machining. In this study FRP chip formation mechanism according to fiber direction and tool shape. Unidirectional composite at various orientations has been investigated that with the use of PCD tool. The fig. 2-2 shows that the fiber orientation and fiber angle θ are determined in the clockwise direction. The cutting tools used for the machining process with the specification clearance angle 7° and rake

angles from 20° to 40° . The reduction of the positive cutting force variation has been observed with a positive fiber directional increase of up to 75° and a high fluctuation in the trimming orientations was occurred greater than 90° .

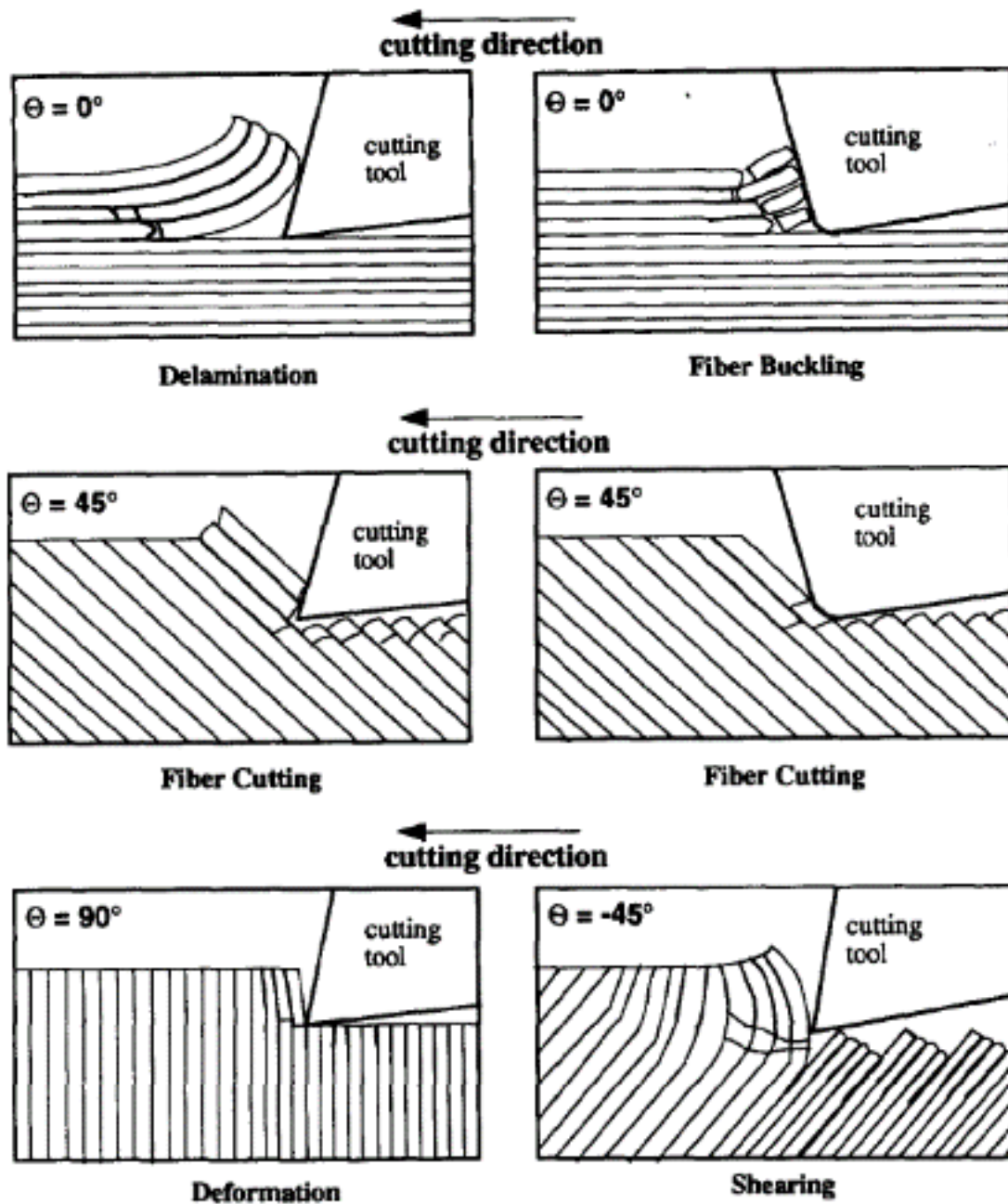


Fig. 2-2. Cutting mechanisms in orthogonal cutting [22]

2.2 Mechanism of the Drilling Process

Drilling is a machining technique used in a milling and drill press to create a circular hole in the workpiece. The chisel region of the drill passes through the small dot hole and chip occurs in the lip region. During this process, friction and force are generated and determine the quality or performance of the drilling process, most drilled hole diameters are larger than the drill diameter, but can also be small, depending on the property of the workpiece. The mechanism of the drilling process includes various variables. In drilling process analysis, the thrust force is the most influential cutting parameters. Bhatnagar *et al.* [23] conducted a shear test to investigate the in-plane shear strength of UD CFRP and proposed cutting force prediction model. Zhang *et al.* [24] used the finite element method to present the cutting of CFRP. To predict the cutting force the cutting zone is divided into three regions. In many metal matrix, composite force prediction models have also been developed in various method. Kishawy *et al.* [25] developed a prediction cutting force model that an energy-based analytical in orthogonal cutting of metal matrix composite. In this paper, the significance of the particle damage mechanism on the cutting performance was discussed and the energy for interfacial debonding was quantified. Pramanik *et al.* [26] developed a mechanic for predicting the forces of cutting metal matrix composite. The cutting force mechanisms are based on the chip formation, matrix ploughing, and particle fracture and displacement.

In this article, to define the mechanism of the thrust force generated by drilling, the force generated by the region of the tool in the orthogonal cutting was obtained and the mechanism for the drilling process was obtained through the coordinate transformation.

2.3 Numerical Studies on Drilling

An orthogonal cutting model that ignores the various complex parts of geometry is an ideal simple model for explaining the mechanism of the cutting process. It is assumed that the orthogonal cutting model works in a completely homogeneous that exclude the concept of heterogeneous deformation. It is assumed that the cutting tool has a straight edge and acts perpendicular to the cutting direction during cutting.

2.3.1 Modelling of CFRP

Numerical studies and simulations of drilling processes for CFRP composites have been widely used by researchers because they can reduce the cost without destruction of the workpiece and drill. With the use of this process, time can be easily reduced in data prediction such as thrust force and internal defects. With these advantages, many researchers have presented a numerical model for CFRP drilling [24,27]. D-M Guo *et al.* [27] developed the numerical of CFRP drilling. The thrust forces and torques of the model were obtained by calculating the forces generated in three areas in orthogonal machining and extended to a three-dimensional drilling model through coordinate transformation. The model emphasizes that cutting forces are a function of all tool geometry and drilling parameters. It is assumed that the thrust force and torque generated in the chisel edge region of the tool simply push the CFRP. The proposed model was successfully incorporated into the geometric parameters and the failure of the matrix. When drilling, high spindle speed and low feed rate result in low thrust forces that go with excellent machining results.

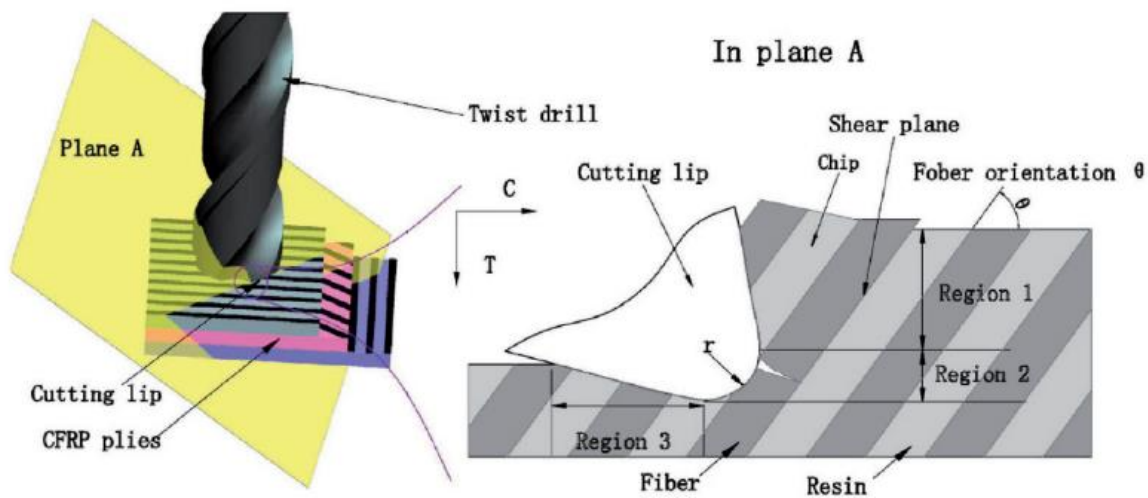


Fig. 2-3. Cross-section on the cutting lip region [27]

Venu Gopala *et al.* [28] developed a FEM model of unidirectional FRP orthogonal cutting. The Coulomb friction law was applied to define the friction between the workpiece and the cutting tool. Tsai-Hill used failure criterion to predict material failure ahead of the chip formation region. The 3D Tsai-Hill criterion was implemented through user subroutine with ABAQUS. The change in stress in the simulation process over time is shown in fig. 2-4.

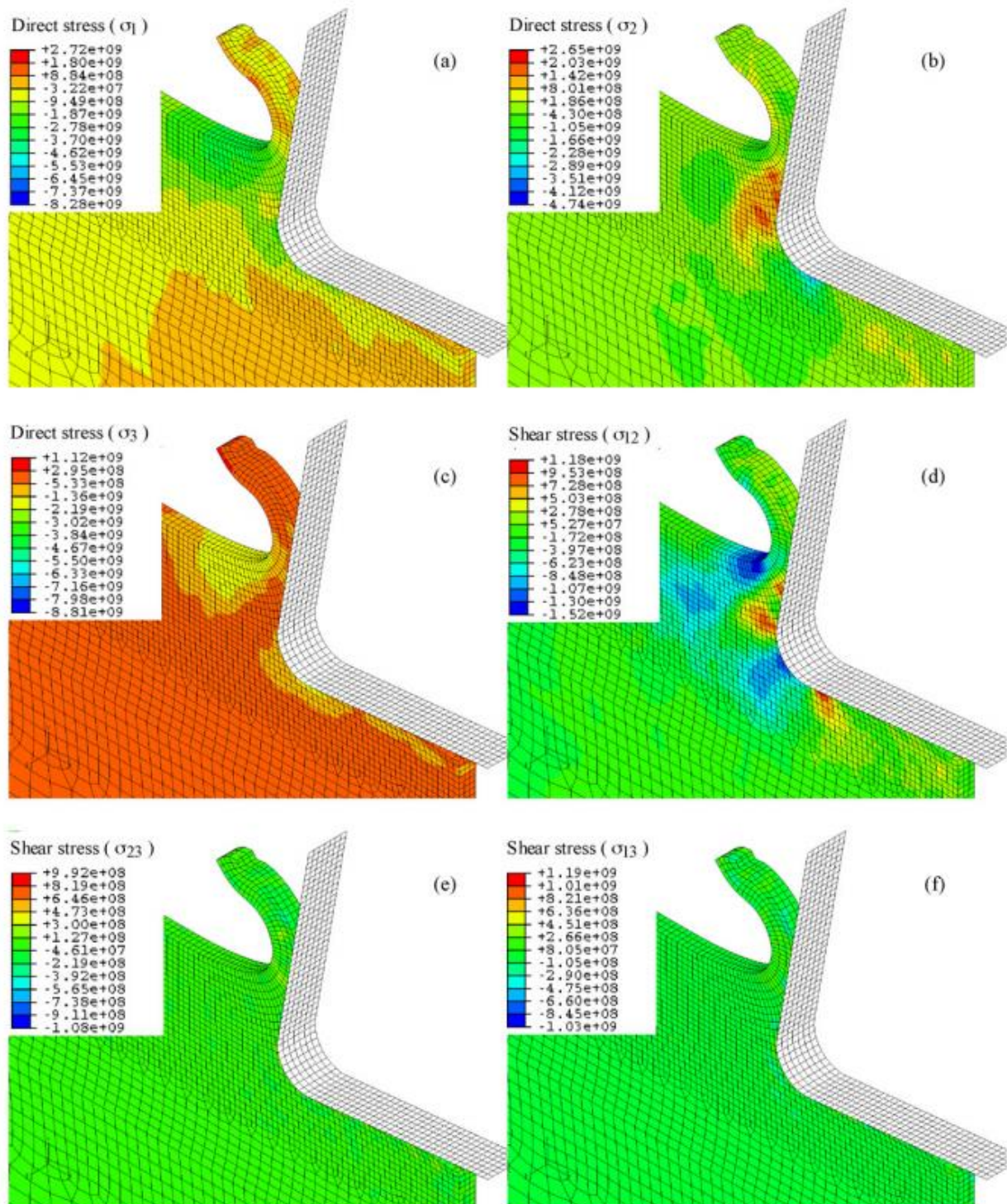


Fig. 2-4. Stresses contour in a workpiece in the case of 0.1mm depth [28]

Durao *et al.* [29] developed a three-dimensional FE model with the study of damage and delamination in fiber reinforced composite. A cohesive damage model was used to represent internal defects. The damage model combines aspects of fracture mechanics stresses and strength-based analysis and failure occur gradually to avoid the singularity at the crack tip. A cylinder-shaped workpiece consisting of 14 element layers modelled. To reduce the time of the simulation, the workpiece consists of 8 layers in which the core region is removed, 4 layers with different orientations according to the stacking sequence and 2 layers with equivalent properties. Shown in the fig. 2-5.

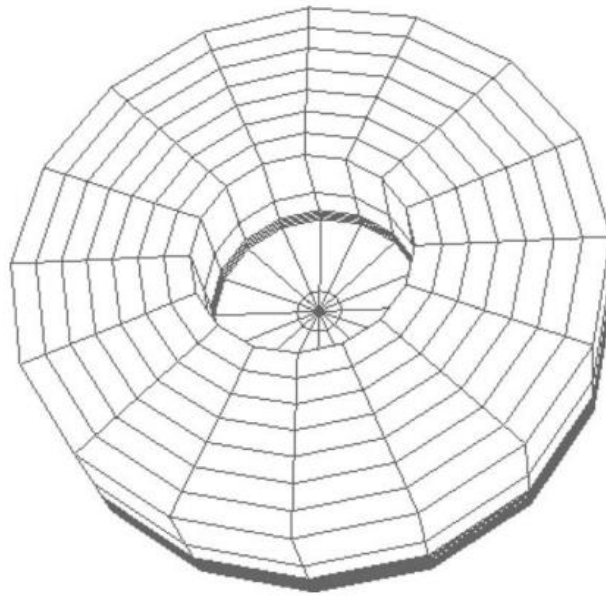


Fig. 2-5. Workpiece model [29]

The drill has composed with the rigid body and the rotation of the tool has not considered concentrating on the process caused by the chisel edge. The results show that the thrust force prediction is accurate, and the main direction of delamination points has consistently 22.5° .

2.3.2 Modelling of Metal

Metal drilling is widely used in machining processes. However, the drilling process requires investigation of tool wear and quality of machined holes [30,31]. In general, the interpretation of general elastic-plastic problems with large deformation in machining is difficult to solve. Numerical models have been widely used to solve these various problems [32]. Drilling process modelling can save time and effort in finding optimal drilling process conditions. Ozden Isbilir *et al.* [33] developed the 3-

dimensional FEM model of titanium alloy drilling. The thrust and torque were predicted by the FEM model. They also used the Johnson-Cook model and the associated damage model to show the configuration behavior of the workpiece under deformation due to cutting conditions. The damage initiated when the equivalent plastic strain has reached the criteria value. Burr height could be predicted through the model based on this critical stress level. With the Von-Mises stress, the stress generated in the workpiece per time and maximum stress and distribution of stress has been predicted as shown in figure 2-6. As a result, the efficiency of the model is shown by comparison with the result through drilling experiment.

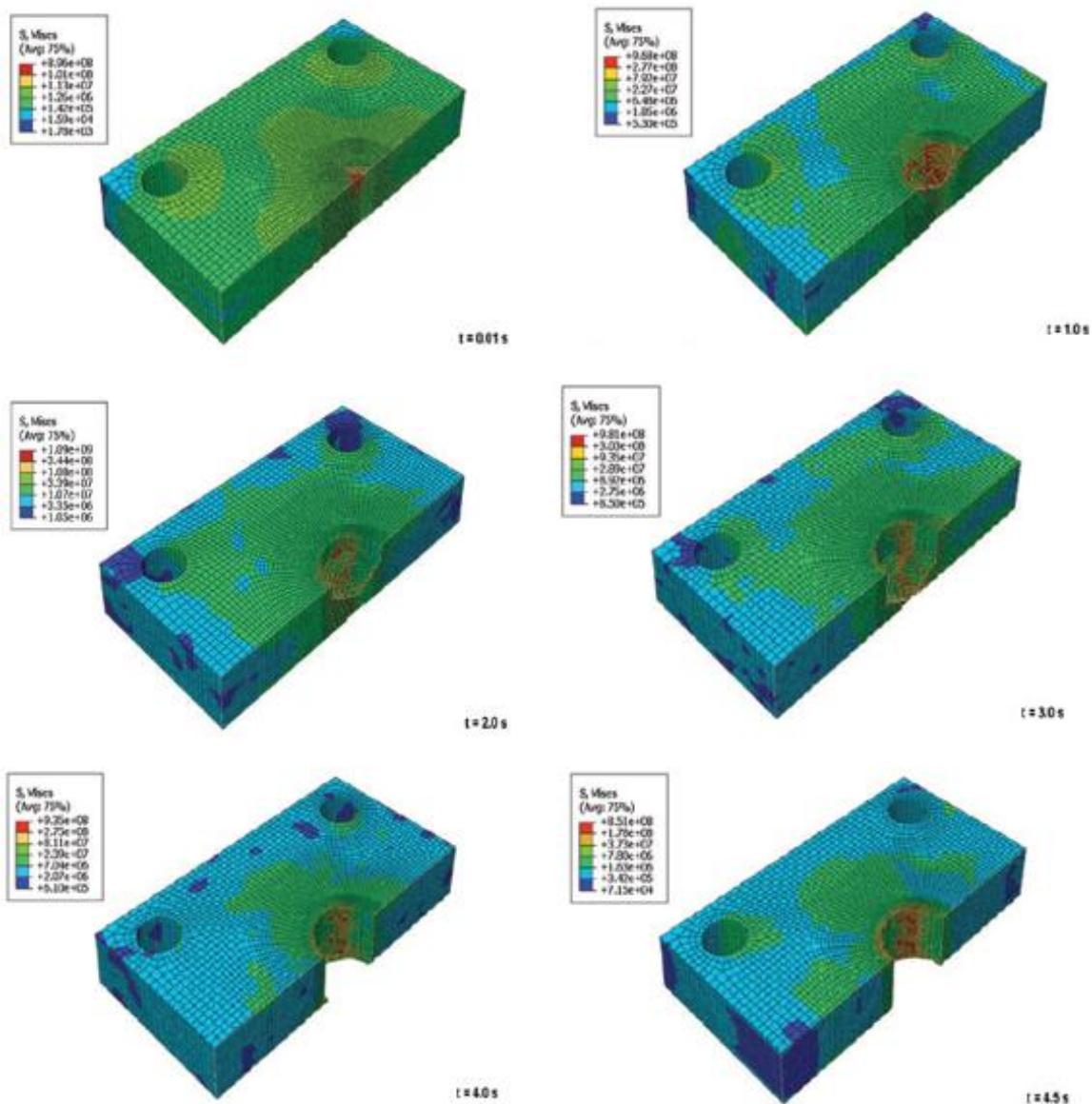


Fig. 2-6. Stress contour of FE model [33]

2.3.3 Modelling of the CFRP-Metal stack

Redouane Zitoune [34] studied cutting parameters of thrust force, torque, hole quality, and chip during CFRP-Al stack drilling. The thrust force and torque measured during drilling were more than two times higher than CFRP in Al part as shown in fig. 2-7. As the diameter of the drill increases the cross-sectional area of the chip increases sharply. Thrust force and torque increased to a higher diameter to a larger chisel edge length. The feed rate and drill diameter can be a cause of internal defects because the change in drill diameter and feed rate affects the change in the cross-sectional area of the chip. On the other hand, the effect of spindle speed seems to be smaller. For all diameters of the tool, the surface delamination increases with an increase in feed rate [35,36].

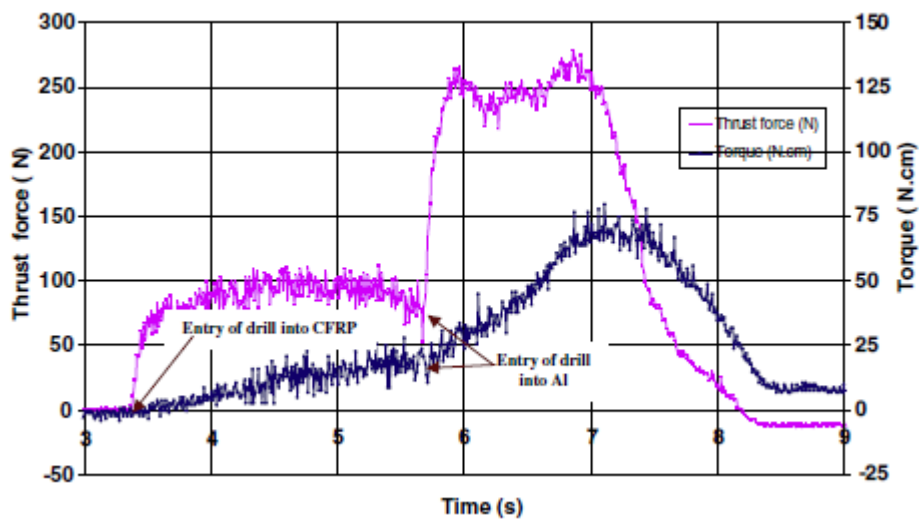


Fig. 2-7. Thrust force and torque in drilling experiment. Diameter = 8 mm, Rotational speed = 1050 rpm and feed = 0.10 mm/rev. [34]

Z. Qi *et al.* [37] developed the three-dimensional FE models to verify the theoretical model of critical thrust force in drilling CFRP-Al stacks. The CFRP layer and the aluminum layer were constructed in the model and the cohesive elements of thickness are zero were constructed between CFRP and aluminum. The cohesive element layer is assumed that the intermediate adhesive material is very thin in the composite material. Critical thrust forces were obtained for each stage to show the conditions under which delamination-free holes were obtained. Figure 2-8 shows that the comparison of the thrust force in the prediction model result and the experimental model result of the drilling process, which is almost similar.

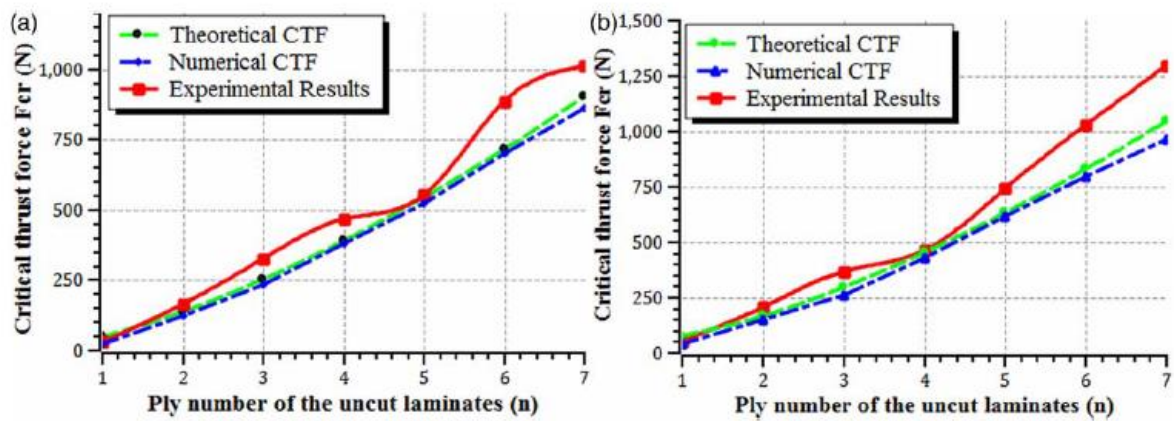


Fig. 2-8. Compare the critical thrust force results (a) Drilling aluminum to CFRP (b) Drilling CFRP to aluminum [37]

S.A Ashrafi *et al.* [38] has experiment under various conditions to investigate thrust, torque and hole quality in the CFRP-Al-CFRP stack drilling process. The thrust force and delamination according to the various feed were investigated. In drilling CFRP-Al-CFRP, increasing feed led to increased entry delamination, higher thrust force and torque, rougher surface on all plates. The second CFRP was less delamination than the first CFRP. This shows that under drilling process conditions where delamination does not occur, it is better to carry out the drilling process with CFRP stacked under metal. Therefore, it is important to find appropriate machining conditions through the thrust force prediction in the CFRP-Al stack drilling process.

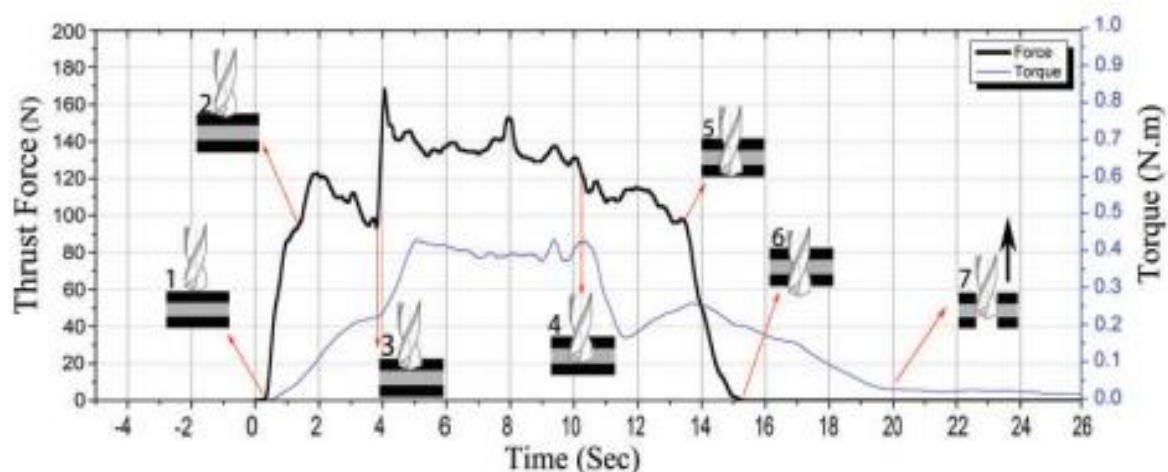


Fig. 2-9. Thrust force and torque in CFRP-Al-CFRP stack drilling process [38]

R. Qi *et al.* [39] investigated the changes in thrust force with machining parameters and drill shapes in the CFRP-Al stack drilling process. The feed rate and drill diameter affect delamination because it affects the increase in cross-sectional area of the chip. On the other hand, the spindle speed has little effect on delamination occurrence. In order to break the chip in the drilling process, the spindle speed should be more than 2020 rpm and the feed rate should be more than 0.1 mm / rev.

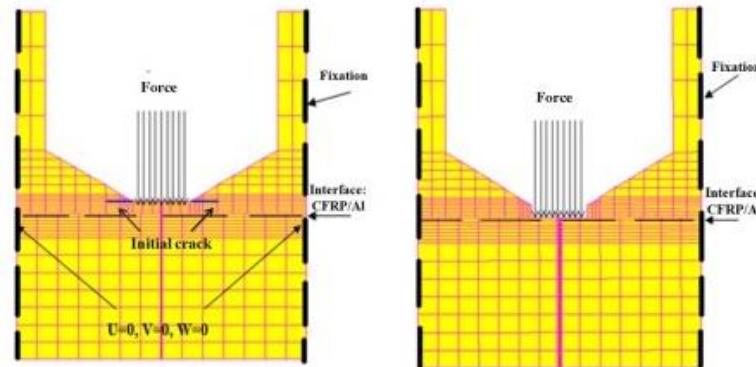


Fig. 2-10. The 3-dimentional model of the CFRP-Al stack [39]

2.4 Summary

In this chapter, we discussed previous researches about CFRP-Al stack cutting mechanisms, drilling and numerical models. The CFRP cutting mechanism was found to be different from the metal along the fiber direction. The most important factor of internal defect in drilling is a critical thrust force and many prediction models are being researched to solve this problem. Therefore, a model for predicting thrust forces is commonly used. Through the thrust force prediction model, optimum machining conditions can be found and machining without internal defects can be performed.

3. PHYSICAL MODEL OF DRILLING IN CFRP-METAL STACK

In this section, the force prediction physical model is introduced. Numerous research has been studied to find optimal cutting conditions to obtain better performance in CFRP-metal stack drilling. Some studies have developed numerical models of critical thrust forces to prevent internal defects in the drilling process. The numerical model is used to find optimal machining conditions in a drilling process with saving time and cost.

3.1 Modelling of the drilling process

The process for completing the physical model can be seen in fig. 3-1. The thrust force generated by drilling was divided into chisel edge and cutting lip region. Based on this, a prediction model was constructed and compared with the experimental results.

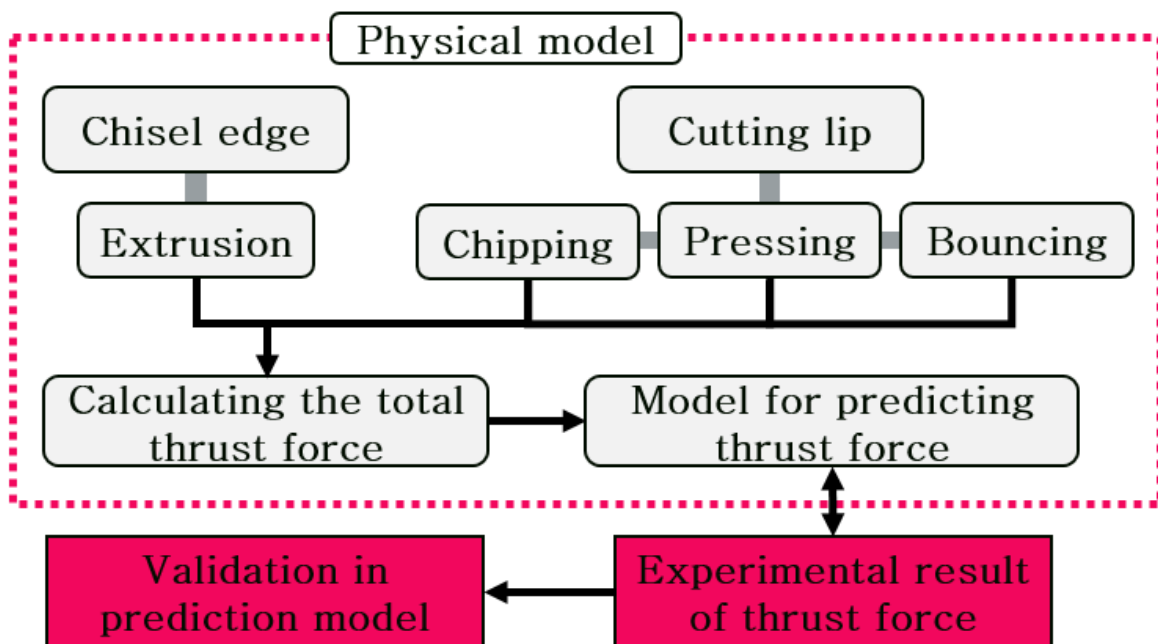


Fig. 3-1. Flowchart for the modelling process

The physical model of drilling in CFRP-Al stack can be divided into six main regions with chisel edge engagement stage, lip region engagement stage, full engagement stage, interface region stage, again full engagement stage and exit stage. This full region is displayed in the figure 3-2.

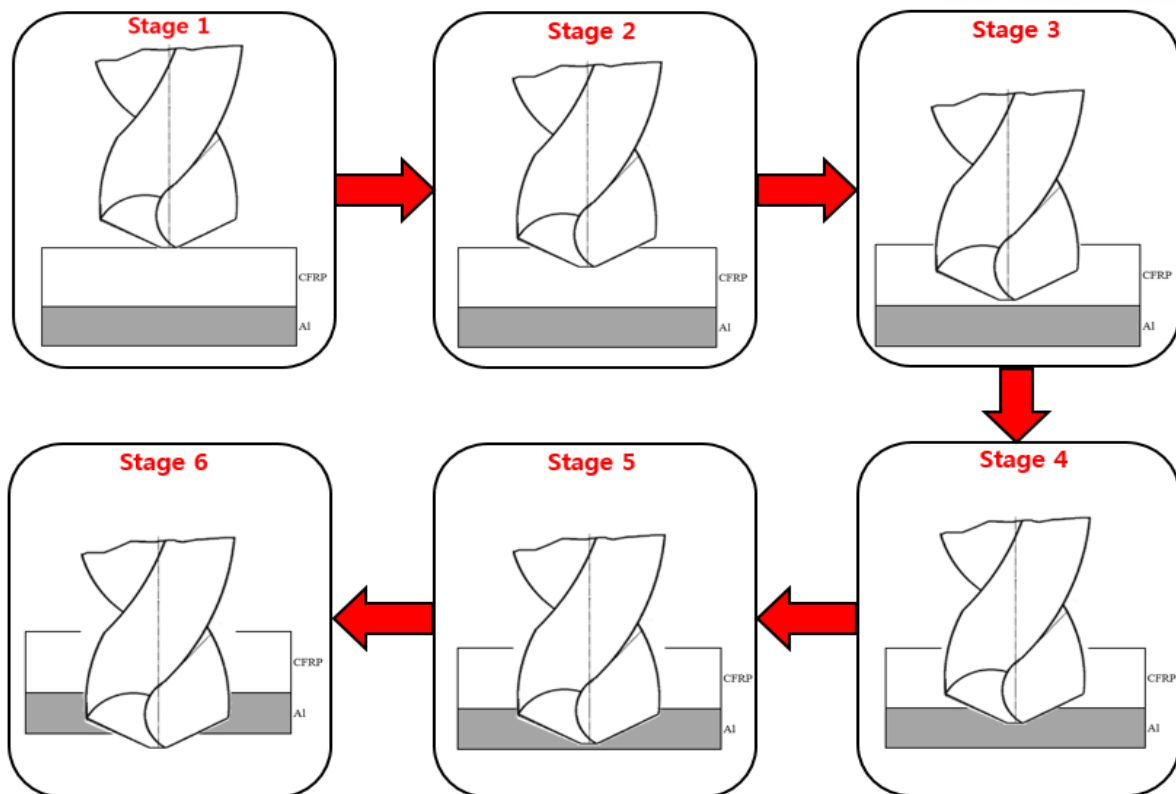


Fig. 3-2. A complete cycle of the drilling process. Chisel edge engagement (Stage 1), lip region engagement (Stage 2), full engagement (Stage 3), interface region (Stage 4), full engagement (Stage 5), exit region (Stage 6).

When chisel edge first starts entering material, the rise in thrust force takes place. This rise continues in force when the lip region also gets engaged in the cutting process. When the lip region of the drill bit engages completely in the cutting process, the rise in thrust force stops. Then the thrust force remains constant until the drill starts to exit from the other end of the material. At the exit stage again decrease in the thrust force takes place until the entire drill bit passes through the entire thickness of the material.

3.1.1 Force formulation in the chisel edge

The chisel edge plays an important role in the drilling process [24,27]. When chisel edge first starts entering material, the rise in thrust force takes place. The force continues to increase until the lip region gets engaged in the cutting process. The force distribution of the cross-section of the chisel edge at A-A and the geometrical parameters are shown in the figure 3-3.

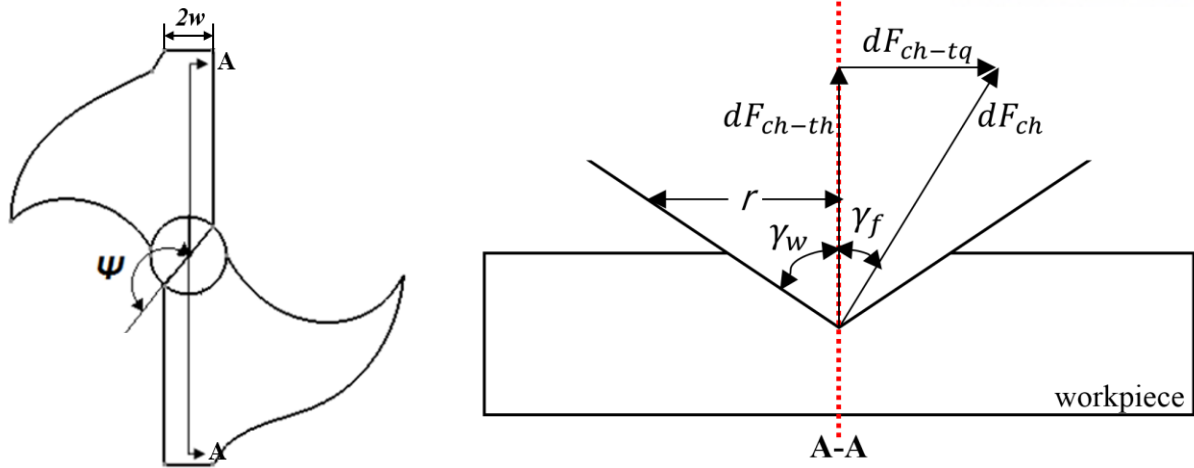


Fig. 3-3. The cutting effect of the chisel edge

Where the $2w$ is the thickness of chisel edge, r is the cutting radius. The elemental cutting force dF_{ch} is consists of two parts; the thrust force generation dF_{ch-th} and the torque generation dF_{ch-tq} . The γ_w is the half of the chisel edge angle, γ_f is the angle between the force of chisel edge and cutting direction.

$$\gamma_f = w / \sin(180 - \psi) \quad (3-1)$$

$$\gamma_f = \tan^{-1}(f/2\pi r_{chi}) \quad (3-2)$$

$$\gamma_w = \tan^{-1}(\tan(\varepsilon_d/2)\sin\psi) \quad (3-3)$$

Where $\varepsilon_d/2$ is the half of the point angle, ψ is the rake angle of the chisel edge.

$$dF_{ch-th} = \frac{E}{1-\nu^2} (k_{ch}w + fnt/2) \tan\gamma_w \cos\gamma_f \quad (3-4)$$

The elementary cutting force can be gotten by chisel edge, where E is Young's modulus of the workpiece, ν is Poisson's ratio, f is the feed rate, n is the rate of rotation, and t is the time in Sec. Therefore, the force by the chisel edge of the workpiece can be represented as follows;

$$F_{ch-th} = \int_{-w/\sin(180-\psi)}^{w/\sin(180-\psi)} \frac{E}{1-\nu^2} (k_{ch}w + fnt/2) \tan\gamma_w \cos\gamma_f dr \quad (3-5)$$

3.1.2 Force formulation in the cutting lip region

To define the thrust force in the lip region, the force generated by the perpendicular cutting system was used [24,40], and it was modelled by transforming it into the drilling coordinate system. The force in the cutting lip region is divided into minute cutting elements. When the cutting element of the cutting lip region is very small, each section of the cutting lip region can be considered as performing orthogonal cutting. The drilling thrust force has been calculated with the concept of orthogonal cutting method. The figure 3-4 shows the cutting effect of lip region and minute cutting element dh can be confirmed. The thrust force F_y in an aluminum can be represented as follows;

$$dF_y = a_c \left(\frac{\gamma_{Al} \cos\phi - \sigma_{Al} \sin\phi}{\sin\phi} \right) dh \quad (3-6)$$

Where a_c is the cutting thickness, γ_{Al} and σ_{Al} are the shear stress and yield stress.

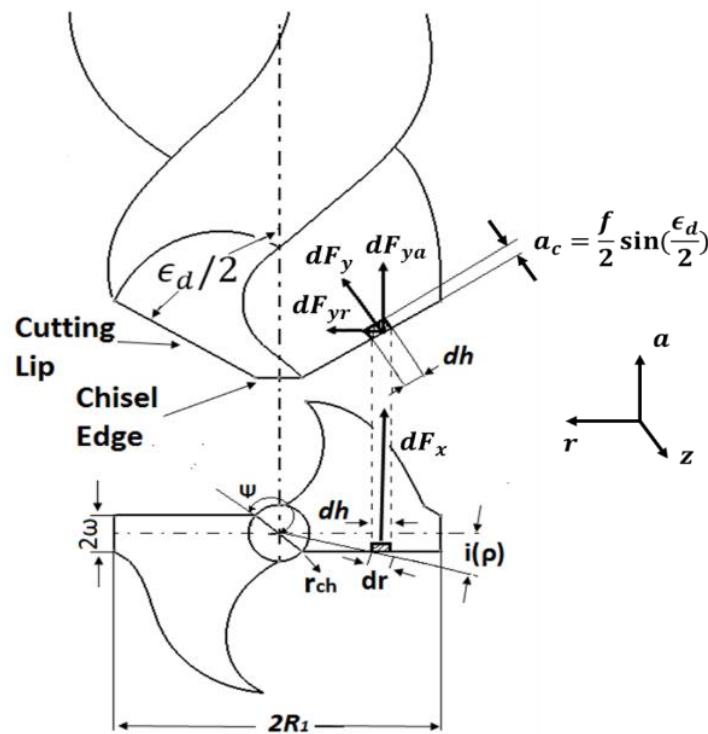


Fig. 3-4. The cutting effect of the lip region

In CFRP cutting, it is different form against aluminum due to the fiber orientation. In the work of Zhang's orthogonal cutting model were used and there are three regions of cutting force generated by the cutting lips [41]. Three regions of orthogonal cutting and force direction can be seen in figure 3-5.

Region 1 – Chipping

The chip occurs during orthogonal cutting. As shown in figure3-4, chipping would be generating the thrust force. The thrust force generates in region 1 is given by dF_{y1} ;

$$dF_{y1} = \frac{\tau_1 a_c \cos \phi \tan(\phi + \beta - \gamma_0) - \sin \phi}{\tau_1 / \tau_2 \cos(\theta - \phi) \sin \theta - \sin(\theta - \phi) \cos \theta} dh \quad (3-7)$$

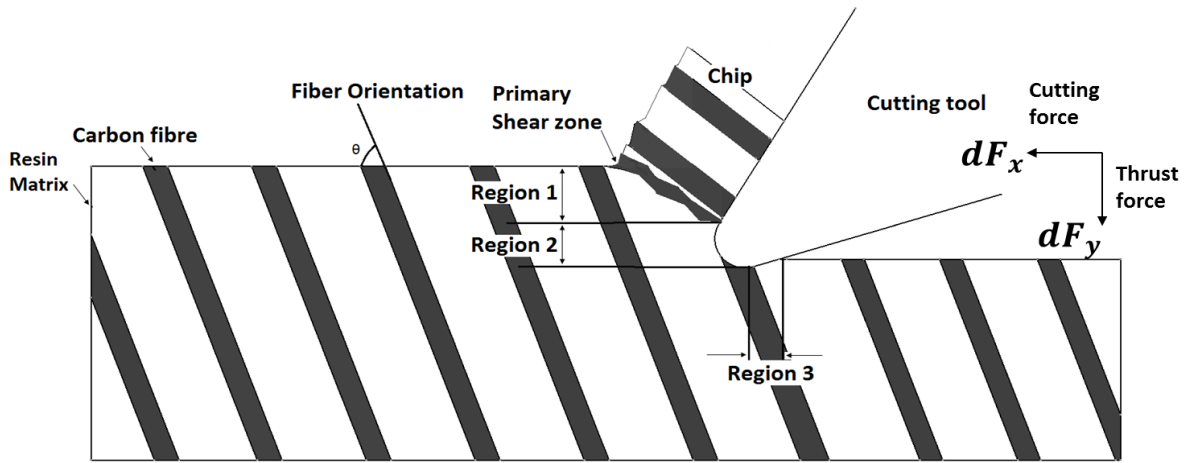


Fig. 3-5. Three regions of the orthogonal cutting

Where τ_1 is the shear strength along the fiber orientation; τ_2 is the shear strength along the fiber orientation; h is the width of a workpiece; a_c is the depth of cut in machining. ϕ is the shear angle of the cutting element of the lip region, θ is the fiber orientation, β is the friction angle and γ_0 is rake angle of the cutting tool. ϕ and γ_0 is represented to calculate the thrust force.

$$\phi = \tan^{-1} \left(\frac{\cos \gamma_0}{1 - \sin \gamma_0} \right) \quad (3-8)$$

$$\gamma_0 = \tan^{-1} \frac{(r \cos \phi_1 \tan \theta_r)}{(R_1 \sin(\frac{\epsilon_d}{2}) - w \cos(\frac{\epsilon_d}{2}) \tan \theta_r)} - \tan^{-1} \left(\frac{\sin \phi_1 \cos(\epsilon_d/2)}{\cos \phi_1} \right) \quad (3-9)$$

Where θ_r is the helix angle of the drill bit varying along the cutting lip region and ϕ_1 is the web angle in the direction normal to the axis of the drill bit.

Region 2 – Pressing

Figure 3-6 show how to analyze the cutting mechanism in Region 2. In region 2 the pressing action takes place by the fillet region of the cutting lip region. In orthogonal cutting, the tool nose presses the workpiece and generate the indentation force. The indentation forces are calculated by adding the force generated in the upper tool nose and lower tool nose. The force is given by P_1 and P_2 as follows;

$$P_1 = \frac{1/2 b_1^2 \pi E^* h}{4 r_e} \quad (3-10)$$

$$P_2 = \frac{1/2 b_2^2 \pi E^* h}{4 r_e} \quad (3-11)$$

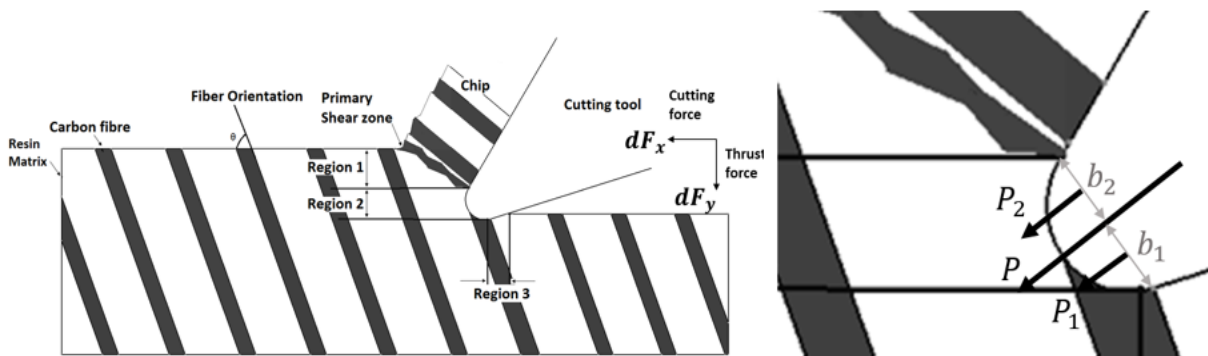


Fig. 3-6. Schematic of CFRP orthogonal cutting in Region 2

Where r_e is tool nose radius; b_1 and b_2 are the widths between tool and workpiece; E^* is the effective elastic modulus and h is the width of the workpiece. Therefore, the indentation force is $P = P_1 + P_2$. The vertical force generated due to the indentation force and given by dF_{y2} ;

$$dF_{y2} = \frac{r_e \pi E}{8(1-\nu_3^2)} (\cos \theta - \mu \sin \theta) dh \quad (3-12)$$

Where r_e is the radius of the fillet in the cutting lip region; μ is the friction coefficient between the workpiece and tool.

Region 3 – Bouncing

In Region 3, the force is generated due to the back of the bouncing phenomenon at the contact region of the tool-workpiece interface. We assume that the back of the bouncing height is the same as the radius of the tool. The vertical force is given by dF_{y3} ;

$$dF_{y3} = \frac{1}{2} r_e E_3 \cos^2 \alpha dh \quad (3-13)$$

Where α is the clearance angle of the tool.

Therefore, the total vertical force can be given as follow;

$$dF_y = dF_{y1} + dF_{y2} + dF_{y3} \quad (3-14)$$

So far, the vertical forces of the orthogonal cutting lip region have been obtained. It should be converted to a drilling force using the orthogonal cutting system. The force dF_y can be transformed into the thrust force component dF_{ya} .

$$dF_{ya} = (dF_{y1} + dF_{y2} + dF_{y3})dh \quad (3-15)$$

In figure 3-7, dh can be represented as Eq. (). If $\rho = r(t)/R_1$ and R_1 is the maximum radius of the drill bit, dh can be represented as Eq. (3-17).

$$dh = \cos(i(\rho)) dr \quad (3-16)$$

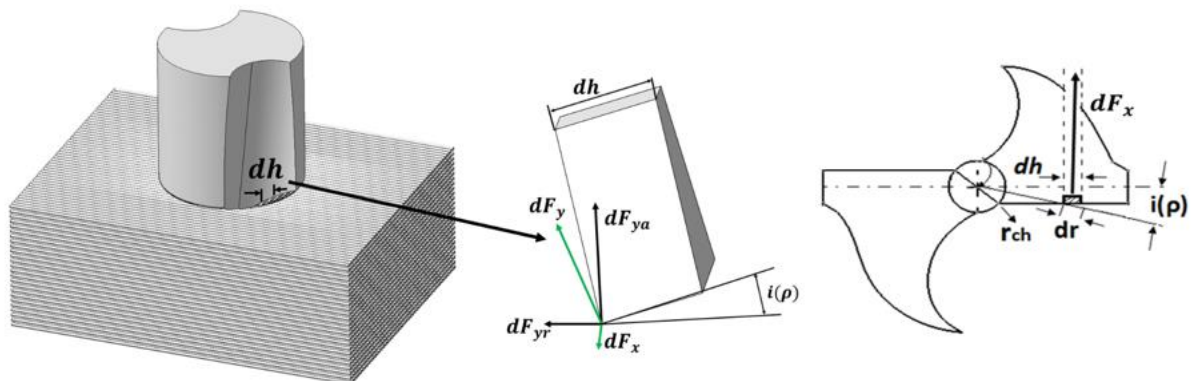


Fig. 3-7. Force transformation for the drilling system

$$dh = \left(1 - \frac{w^2 \sin^2\left(\frac{\epsilon_d}{2}\right)}{2\rho^2 R_1^2}\right) R_1 d\rho \quad (3-17)$$

Where $i(\rho)$ is the inclination angle. Taking from equation 3-17 for Al and CFRP, the thrust force equation on cutting edge, both aluminum and CFRP can be represented as follow;

$$dF_{Al} = \left(\frac{\gamma_{Al} \cos\phi - \sigma_{Al} \sin\phi}{\sin\phi}\right) \left(1 - \frac{w^2 \sin^2\left(\frac{\epsilon_d}{2}\right)}{2\rho^2 R_1^2}\right) R_1 d\rho \quad (3-18)$$

$$dF_{CFRP} = (dF_{y1} + dF_{y2} + dF_{y3}) \left(1 - \frac{w^2 \sin^2\left(\frac{\epsilon_d}{2}\right)}{2\rho^2 R_1^2}\right) R_1 d\rho \quad (3-19)$$

Now by applying the limit, the force in lip region can be shown as follow;

$$F_{lip-Al} = 2 \int_{a_1}^{b_1} dF_{Al} \sin\left(\frac{\epsilon_d}{2}\right) \quad (3-20)$$

$$F_{lip-CFRP} = 2 \int_{a_1}^{b_1} dF_{CFRP} \sin\left(\frac{\epsilon_d}{2}\right) \quad (3-21)$$

The limit of the integration for the equation is dependent on the effective radius of the chisel edge and the drill bit. As seen in figure 3-8, the radius increases until it reaches a maximum value R_1 at the beginning and then remains at R_1 . The time-dependent parameter $r(t)$ is shown as follow;

$$r(t) = \sqrt{\left(\frac{w}{\sin(180 - \phi)}\right)^2 + \Delta^2 + 2w\Delta/\sin(180 - \phi)\sqrt{1 - \sin^2(180 - \phi)}} \quad (3-22)$$

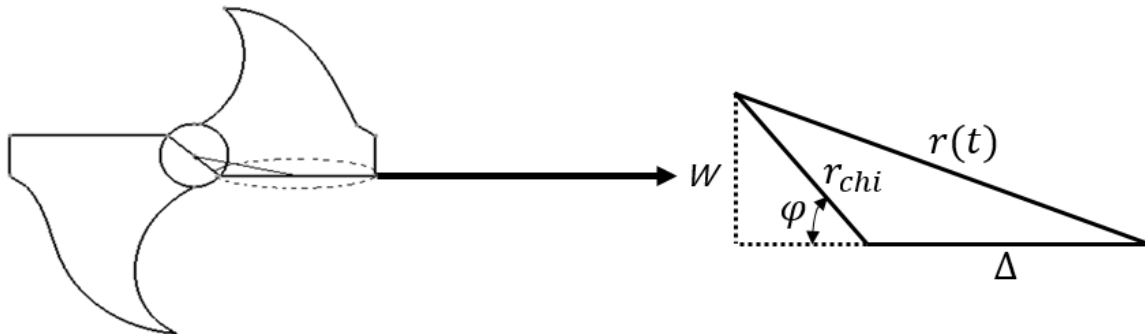


Fig 3-8. Change in cutting radius over time.

Where r_{chi} is the initial cutting length, $r(t)$ is the max length at time t , Δ is the time-dependent increment and simplified as $\Delta = \frac{fnt}{\cos(\epsilon_d/2)}$ and will remain as R_1 after reaches a maximum value of limit a_1 and b_1 are given by the equation as follow;

$$a_1 = \frac{w}{R_1 \sin \phi} = \frac{r_{chi}}{R_1} \tag{3-23}$$

$$b_1 = \frac{r(t)}{R_1} \tag{3-24}$$

Assuming θ_0 is the fiber orientation of the cutting CFRP and $i(\rho)$ is the inclination angle, the equivalent fiber orientation can be represented as follow;

$$\theta = \cos^{-1} \cos(\theta_0) \cdot \cos i(\rho) \tag{3-25}$$

3.2 Material property

Carbon fiber composite materials namely USN 150E was used for the model. It was cured using autoclave at 125-degree C for 90 minutes under 5bar pressure. The detailed parameters for the CFRP composites are displayed in table 3-1. The material properties of the CFRP composite were calculated using the rule of mixture. And parameters of Aluminum for the model are displayed in table 3-2.

Table 3-1. Parameters of CFRP

E_1	$E_2 = E_3$	τ_1	τ_2	ν_{13}
166GPa	10.13GPa	99Mpa	75Mpa	0.28

Table 3-2. Parameters of Al

E_{Al}	σ_{Al}	τ_{Al}	ν_{Al}	Density
70GPa	445MPa	150Mpa	0.34	2.8g/mm ³

3.3 Summary

In this chapter, the physical model for CFRP-Al stack drilling was established. To obtain the thrust force, the forces generated in the chisel edge region and the lip region of the tool were obtained at orthogonal cutting. The total thrust force was obtained as the sum of the thrust force values obtained at each part. The thrust force obtained from two dimensions was applied to 3-D drilling process through coordinate transformation. In the CFRP-Al stack drilling process, total 6 stage Chisel edge engagement (Stage 1), lip region engagement (Stage 2), full engagement (Stage 3), interface region (Stage 4), full engagement (Stage 5), Exit region (Stage 6) were divided and the thrust force values at each stage were obtained. The experiment of CFRP-Al drilling was performed to verify the prediction force model with the results of the experiment.

4. FINITE ELEMENT MODEL OF DRILLING IN CFRP-METAL STACK

In this chapter, the finite element model is introduced. The thrust force of the drilling process and the internal defect will be shown by this prediction model. To obtain excellent performance in CFRP-Al Stack drilling process, many studies have been performed to optimize cutting conditions. Understanding the CFRP-Al stack cutting conditions for defect reduction is important. One of the biggest reasons for internal defects in the critical thrust force because the thrust force value is determined by the processing condition. Therefore, a numerical model of drilling machining considering cutting force has been developed by many researchers.

In this article, the ABAQUS software has been used for predicting modelling. The Finite Element Method (FEM) is not limited to boundary conditions and can be interpreted in a continuum of various composites. It also provides a system for properly modelling the CFRP-Al stack drilling process within a reasonable computation time and developing an analytical model that can predict the level of thrust force and delamination failure.

4.1 FE model setup

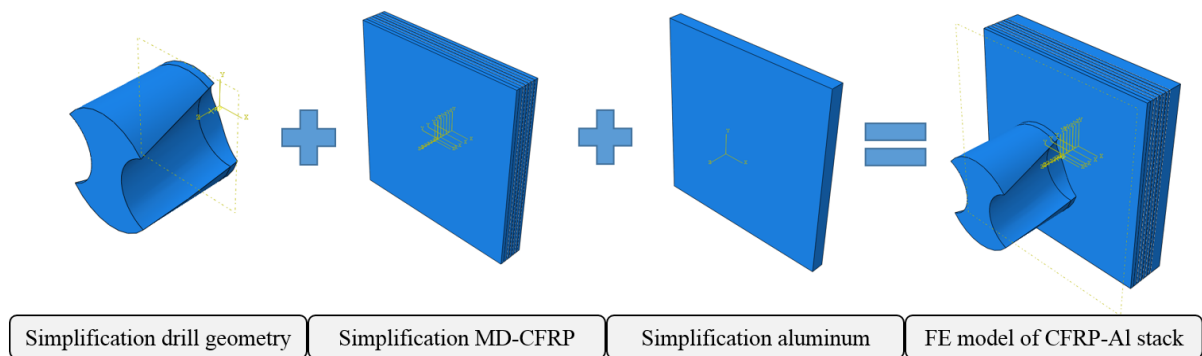


Fig 4-1. The progress of CFRP-Al Stack drilling

The model presented in this paper uses ABAQUS / Explicit software. ABAQUS / Explicit, which can be used for dynamic analysis in a relatively short time, is suitable for drilling. It was also possible to interpret effectively the problem of discontinuous behavior including complex contact conditions. Figure 4-1 shows the CFRP-Al STACK drilling process for 3D FE modelling. This model

predicts the thrust force during the drilling process and estimates the delamination failure and the degree of internal stress. The goal of this model is to simulate the drilling process of CFRP-Al Stack.

4.1.1 Geometry modelling and boundary conditions

The drilling model is shown in Figure 3-2. The geometry is consisting of CFRP with 3cm and aluminum with 2cm. CFRP is composed of 7ply in total to see internal defect and stress distribution according to the drilling process. Considering the multi-direction CFRP, each layer is composed of intersections of 0° and 90° , and the total size is $20\text{ mm} \times 20\text{ mm}$. The bonding process between CFRP layers and between CFRP and Al, the cohesive conditions were used, and the thickness was assumed to be zero because it was used for bonding. In the experimental and FE model, a drill with a diameter of 9 mm and a helix angle of 30° with a point angle of 135° was used. To reduce the calculation time of simulation, the drill has been drawn to simplify with reasonable element size. Also, the effect on drill wear was not taken into the model to reduce the calculation of simulation time. The drill was set to the rigid body and the reference point was located at the endpoint of the drill.

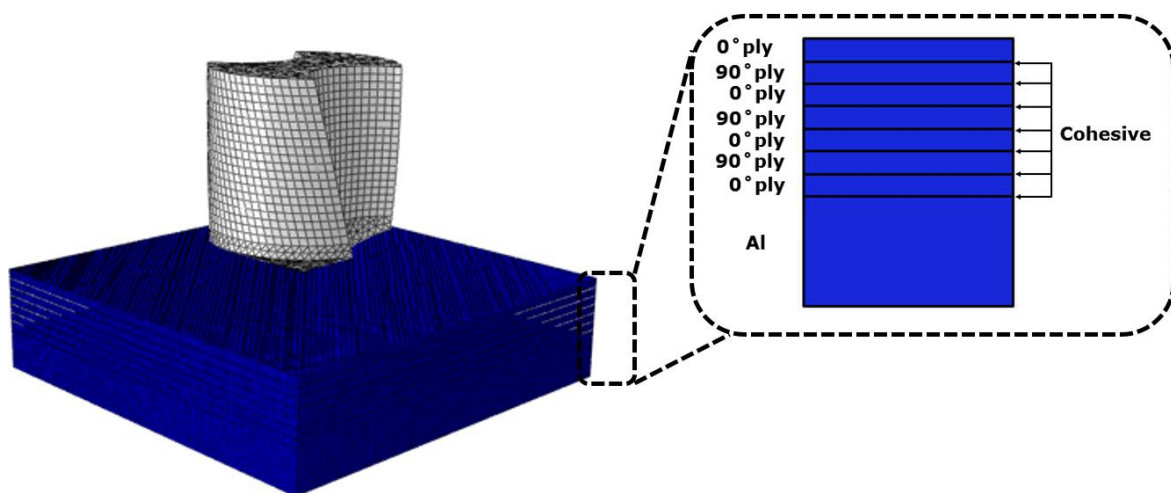


Fig 4-2. FE model geometry

The boundary conditions of the FE model are set as shown in Figure 4-3. In the experiment, the fix condition has been given to the whole part except the part where the drill was machined. In this model used the velocity boundary condition at the reference point which defines the feed rate during the experiment.

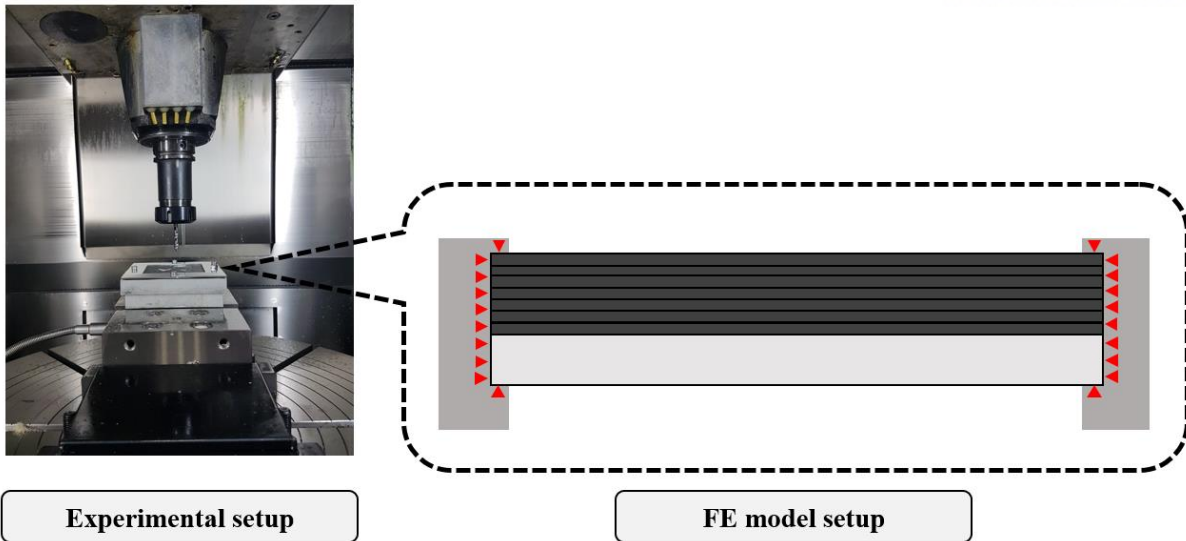


Fig 4-3. Boundary condition of the FE model

4.1.2 Finite elements and mesh type

It is important to follow as possible the experimental conditions when modelling and meshing FE models. Mesh size and shape require proper selection because it reduces computation time and affects the precision of the results in simulation. For the CFRP the element type C3D8R is used for mesh it represents as the hexahedron shape with eight-node linear brick elements. The mesh size of the element is $0.15\text{mm} \times 0.15\text{mm} \times 0.15\text{mm}$ has been used in multi-direction CFRP. For the aluminum plate modeled, the brick elements were used, and the mesh type was C3D8R i.e. 8-node linear brick. Its global size was 0.3 in the aluminum plates. Finally, the drill part was divided into two parts to reduce the computation time. The mesh type of the drill was 3-node triangular shape and C3D6, which was a 6-node linear-triangular, and it was refined with global size: 0.39 elements the part 1 of drill parts. The mesh type of part 2 was rectangular shape: the swept type, which was defined by global size: 0.39 elements to reduce the computing time in part 2. The element of the model can be seen in figure 4-4.

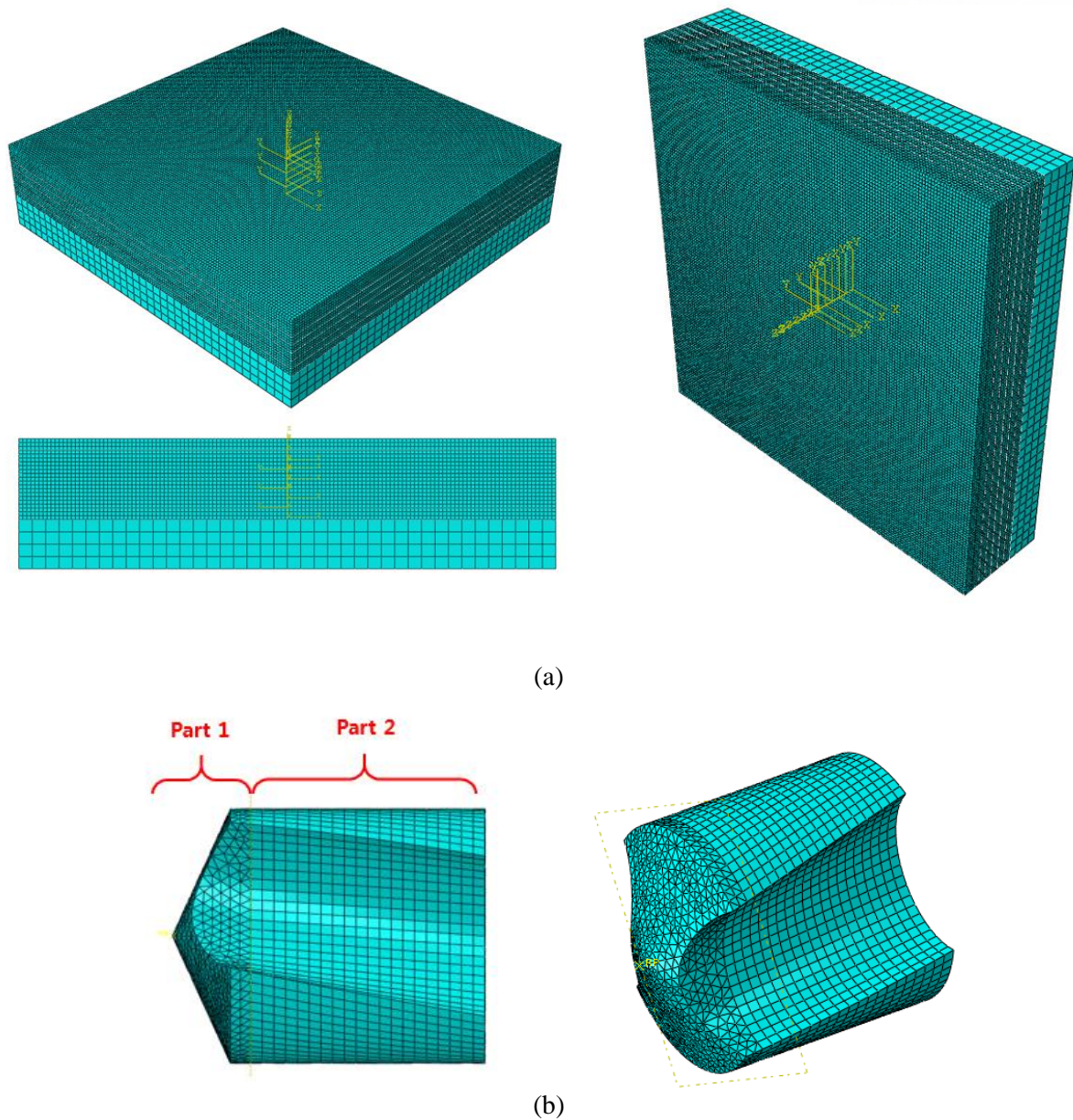


Fig. 4-4. Mesh of FE model (a) CFRP-Al stack, (b) Drill bit

4.2 Material property

The simulated CFRP-Al stack was composed of multi-directional (MD) carbon fiber reinforced plastics and aluminum alloy (Al-6061) as discussed in subsection 4.1. Table 4-1, 4-2 shows the material properties of CFRP and aluminum.

Table 4-1. Material properties of the CFRP

E_{11}	$E_{22}=E_{33}$	$\nu_{12}=\nu_{13}$	ν_{22}	$G_{12}=G_{23}$	G_{13}	ρ
131GPa	7.7GPa	0.	0.	3.5GPa	2.7GPa	1600kg/m ³

Table 4-2. Material properties of the Al6061

Density (ρ)	Young's modulus (E)	Poisson's ratio (ν)
27kg/m ³	7000GPa	0.33

Table 4-1 shows the Elastic properties of MD CFRP that involved the values of fracture for interlaminar damage. Damage evolution was based on the Power law in mixed-mode. Between the plies of the model, the cohesive zones were inserted to simulate delamination. Between the drill and the CFRP-Al stacks, the general contact with appropriate properties in ABAQUS/explicit was defined.

4.2.1 Aluminum modelling

The material behavior of Al 6061 alloy was assumed to be isotropic and elastic-plastic. In the ABAQUS/Explicit software program using the isotropic plasticity model is available. In the FE model for drilling under various conditions, the simulation under similar conditions of the experimental environment is necessary. The FE model of this paper in aluminum part adopts the constitutive model proposed by Johnson-Cook. This model satisfactorily represents the ductile behavior in consideration of the large strain occurring during processing. The material used in this study is Al-6061 alloy. Components of the Johnson–Cook's relationship between flow stress $\bar{\sigma}$, strain rate $\dot{\epsilon}$ and temperature T , is represented by equation (4-1) [42,43].

$$\bar{\sigma}=(A+B\bar{\epsilon}^n)\left(1+C \ln \frac{\dot{\bar{\epsilon}}}{\dot{\bar{\epsilon}}_0}\right)\left[1-\left(\frac{T-T_r}{T_m-T_r}\right)^m\right] \quad (4-1)$$

Where $\bar{\epsilon}$ is the effective plastic strain, $\dot{\bar{\epsilon}}$ the effective plastic strain rate, $\frac{\dot{\bar{\epsilon}}}{\dot{\bar{\epsilon}_0}}$ the normalizing strain rate and A, B, C, m and n are material constants. The parameter n considers the effect of strain hardening, and m models the thermal softening effect. The constant C represents the strain rate sensitivity. The parameter of Johnson-Cook material constants for Al-6061 alloy is displayed in table 4-3.

Table 4-3. Johnson-Cook material constants for Al-6061 alloy

$A(\text{Mpa})$	$B(\text{Mpa})$	$C(\text{Mpa})$	n	m
321.4	113.8	0.002	0.42	1

To simulate the damage initiation in Al-6061, the Johnson-Cook ductile damage criteria was used in ABAQUS/Explicit. The Johnson-Cook failure model which contains five failure parameters was used as a damage initiation criterion and it is presented in equation (4-2). In Johnson-Cook failure model, a scalar damage parameter ω reaches 1 than damage initiation is assumed to happen. The ω is depended on a cumulative law as shown in equation (4-3). The equivalent plastic strain at the onset of damage $\bar{\epsilon}_i$ is presented as follows.

$$\bar{\epsilon}_i = \left[D_1 + D_2 \exp(D_3 \frac{P}{\bar{\sigma}}) \right] \left(1 + D_4 \ln \frac{\dot{\bar{\epsilon}}}{\dot{\bar{\epsilon}}_0} \right) \left[1 + D_5 \left(\frac{T - T_r}{T_m - T_r} \right) \right] \quad (4-2)$$

$$\omega = \sum \frac{\Delta \bar{\epsilon}}{\bar{\epsilon}_i} \quad (4-3)$$

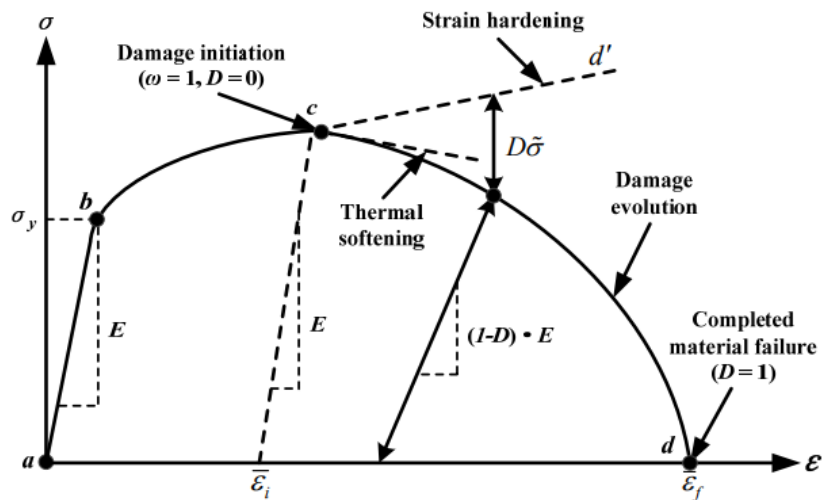


Fig. 4-5. Strain-stress relationship of ductile material failure process [42]

Where $\bar{\varepsilon}_i$ is the equivalent plastic strain at damage initiation, D_1 , D_2 , D_3 , D_4 and D_5 are failure parameters that used to calculate the damage of material, P is the pressure stress and $\bar{\sigma}$ is the Mises equivalent stress. ω is the scalar damage parameter and $\Delta\bar{\varepsilon}$ is the equivalent plastic strain increment. The Johnson-Cook constitutive material property and damage model parameters D_1 to D_5 of Al 6061 alloy are shown in table 4-4. The damage evolution defines the behavior of the material after damage initiation and calculates the rate of material stiffness degradation when the stress-based damage-initiation criterion is satisfied.

Table 4-4. Johnson cook damage model parameters for Al6061

D_1	D_2	D_3	D_4	D_5
-0.77	1.45	-0.47	0.01	0

When metal is damaged, the stress-strain relationship no longer represents the behavior of the material and depending on the location of the deformations will result in strong mesh dependency. To reduce mesh dependency, Hillerborg's fracture energy criterion was used [45]. Hillerborg defined the energy needed to open a unit area of the crack (G_f), as a material parameter. The fracture energy is represented as the following equation.

$$G_f = \int_{\bar{\varepsilon}_i}^{\bar{\varepsilon}_f} L \sigma_y d\bar{\varepsilon} = \int_0^{\bar{u}_f} \sigma_y d\bar{u} \quad (4-4)$$

Where $\bar{\varepsilon}_i$, $\bar{\varepsilon}_f$ are the equivalent plastic strain at damage initiation and failure respectively. L defines the characteristic length, σ_y denotes the yield stress. $\bar{\varepsilon}$ is the equivalent plastic strain, \bar{u}_f is the equivalent plastic displacement at failure and \bar{u} is the equivalent plastic displacement. The damage evolution of the variable with the plastic displacement D is used with linear form. With plastic displacement, it assumes a linear evolution of the damage variable. The damage variable increases as shown in equation (4-5).

$$D = \frac{L\bar{\varepsilon}}{\bar{u}_f} = \frac{\bar{u}}{\bar{u}_f} \quad (4-5)$$

The equivalent flow stress of the material at a given time during FE calculation is given by the following equation.

$$\bar{\sigma} = (1 - D)\tilde{\sigma} \quad (4-6)$$

If $D=D_{max}$ the element is removed from the mesh. Also, when D reaches maximum degradation, no more damage is accumulated on the integration point.

4.2.2 CFRP damage modelling

In the processing of fiber-reinforced composite materials, damage plays an important role. Since many materials exhibit elastic-brittle behavior, damage begins without significant plastic deformation. As a result, plasticity can be neglected when modelling the behavior of brittle materials. [46]. The damage usually occurs perpendicular to the fiber direction. Finally, cracking damage occurs because of the propagation through the fiber cross-section. The FE model in this paper predicts the failure as well as damage of CFRP. Failure and damage begin with homogeneous fly properties depending on the characteristic of the interaction and laminate layup. This method of modelling the gradual failure of composites offers several advantages. Firstly, 3-dimensional stress conditions can be considered, which are limited to 2-dimensional stress states. Secondly, the damage can be found by element removal in ABAQUS/explicit. When the element receives a certain amount of force, the element was able to eliminate. In this method, inter-ply damage of a complex structure can be easily seen. For this damage model, the initiation criteria are based on Hashin's theory [47] in which the failure surface is expressed in the effective stress space. These criteria consider fiber tension, fiber compression, matrix tension, and matrix compression for four different damage initiation mechanisms. The damage model was used to the theory of Puck and Schurmann that has shown the predictive for several failure criteria in composite layers [48, 49]. In this study, the Hashin's criteria were adopted to estimate fiber damage, and the Puck's failure criteria were utilized to the matrix failure model. The algorithm of VUMAT ABAQUS/explicit was presented in figure 4-6.

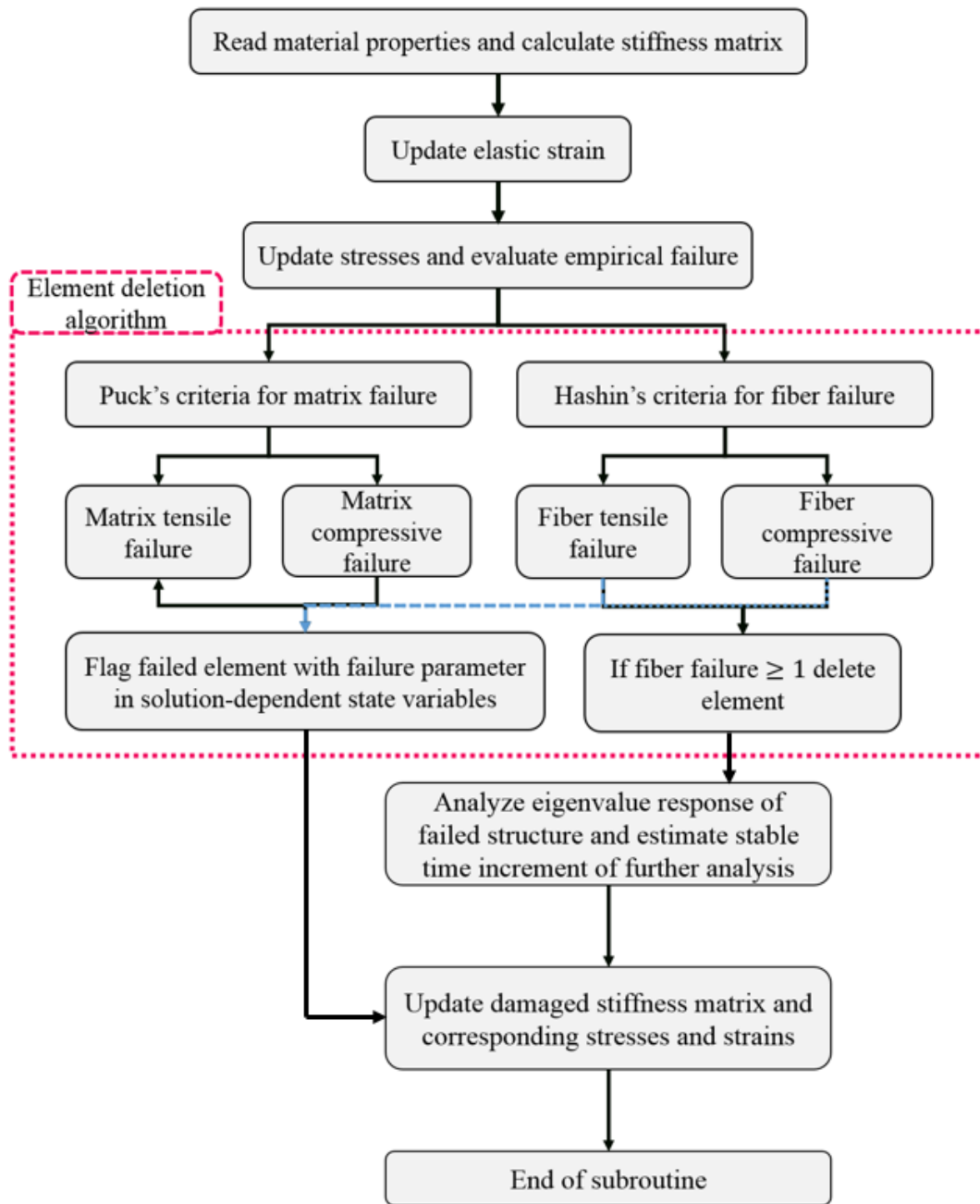


Fig 4-6. The algorithm of VUMAT ABAQUS/Explicit [50]

According to elastic fibers Hashin's criteria for failure

Fiber tensile failure ($\sigma_{11} \geq 0$)

$$\left(\frac{\sigma_{11}}{S_{11}}\right)^2 + \left(\frac{\sigma_{11}}{S_{12}}\right)^2 + \left(\frac{\sigma_{11}}{S_{13}}\right)^2 = 1, \quad d_{ft} = 1 \quad (4-7)$$

Fiber compressive failure ($\sigma_{11} < 0$)

$$\left(\frac{\sigma_{11}}{X_{1c}}\right)^2 = 1, \quad d_{fc} = 1 \quad (4-8)$$

In brittle epoxy matrix Puck's criteria for failure

Matrix failure

$$\left(\frac{\sigma_{11}}{2X_{1t}}\right)^2 + \frac{\sigma_{22}^2}{|X_{1t}X_{1t}|} + \left(\frac{\sigma_{12}}{S_{12}}\right)^2 + \sigma_{22} \left(\frac{1}{X_{2t}} + \frac{1}{X_{2c}}\right) = 1 \quad (4-9)$$

$$\sigma_{11} + \sigma_{11} > 0, \quad d_{mt} = 1$$

$$\sigma_{22} + \sigma_{33} < 0, \quad d_{mc} = 1$$

Where σ_{11} , σ_{22} , σ_{33} and σ_{12} are the stress tensors at an integration point of an element. d_{ft} , d_{fc} , d_{mt} and d_{mc} are the damage variables related to failure modes in fiber tension and matrix compression. X_{1t} and X_{2t} are tensile failure stresses, and tensile failure stress in fiber direction and X_{2c} is compressive failure stress in direction 2, and S_{11} , S_{12} and S_{13} are shear failure stresses. The parameters for strength in MD-CFRP used in this FEM model are presented in table 4-5.

To remove the elements in drilling FE analysis the mesh of element was used to the value of damage variables from the equation (4-7) to the equation (4-9), which was used to distinct damage modes in the modelling CFRP materials. The element was removed when the condition of the maximum damages reaches all the points of some integration point area. The damage value, d ($d \in \max\{d_{ft}, d_{fc}, d_{mt}, d_{mc}\}$), was defined when $d=1$, the element deletion from the mesh occurs. It means that no more resistance to deformation in the model [51].

Table 4-5. Strength properties of Multi-direction CFRP.

$X_{1t}=X_{2t}$	X_{3t}	$X_{1c}=X_{2c}$	X_{3c}	S_{12}	$S_{13}=S_{23}$
840MPa	50MPa	570MPa	70MPa	72MPa	100MPa

4.3 Delamination modelling

In the FE model, the delamination was modelled using cohesive condition available in ABAQUS/explicit. The damage of cohesive elements was modelled with a bilinear traction–separation. The criteria based on normal and shear stresses when the delamination initiated is defined as the following equation (4-10).

$$\left[\frac{t_n}{t_n^0}\right]^2 + \left[\frac{t_s}{t_s^0}\right]^2 + \left[\frac{t_t}{t_t^0}\right]^2 = 1 \quad (4-10)$$

Where t_n , t_s and t_t are the normal stress and the shear traction at the cohesive interface respectively. And t_n^0 , t_s^0 and t_t^0 are defined as the maximum values of normal stress when the deformation is begun [52].

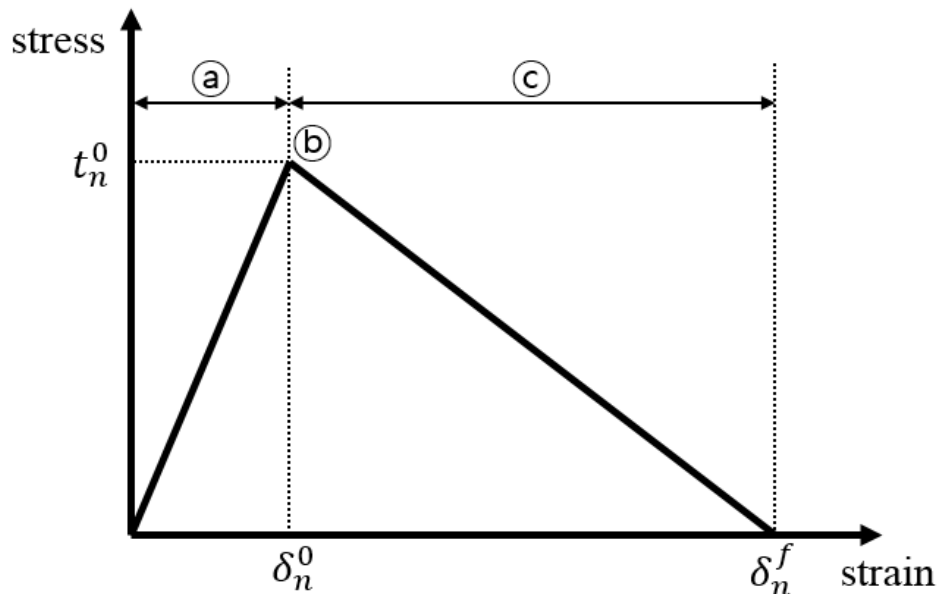


Fig. 4-7. Damage criterion and evolution in the interface cohesive

The power law fracture criterion was used to the fracture energies which was based on mixed-mode. The fracture energy can be expressed with the following equation:

$$\left[\frac{G_n}{G_n^c}\right]^\beta + \left[\frac{G_s}{G_s^c}\right]^\beta + \left[\frac{G_t}{G_t^c}\right]^\beta = 1 \quad (4-11)$$

Where G_n , G_s and G_t are the immediate fracture energies in normal and shear directions, and G_n^c , G_s^c and G_t^c are the critical values of the fracture energies required to initiate failure in the normal, the first and the second shear directions, respectively. The interface cohesive was defined by a traction-separation law with mode-I and the failure is described in the figure 4-7.

In figure 4-7 the part (a) shows linear elastic behavior by the stiffness of the normal and the two shear directions (K_n , K_s and K_t), and it constantly increases to the maximum value of the normal stress. At this part, damage does not occur. Point (b) describes damage initiation criterion, and its required traction stresses in the interface are nominated as t_n , t_s and t_t . Part (c) is the damage evolution by the critical fracture energy (G_n^c , G_s^c and G_t^c), and this part reveals stiffness degradation resulting from the damage evolution. The cohesive properties were given in table 4-6.

Table 4-6. Material properties used in cohesive of the interface.

K_n	$K_s=K_t$	G_n^c	$G_s^c=G_t^c$	t_n	$t_s=t_t$	β
1GPa	1GPa	0.2N/mm	1N/mm	30MPa	60MPa	1

4.4 Summary

In this chapter, the FE model for CFRP-Al stack drilling was established. Simulation of the drill and CFRP-Al stack constructed in the FE model and simulations were carried out with boundary condition between drill and workpiece. To improve the model efficiency in the analysis, the optimal mesh shape was determined. VUMAT in the 3D CFRP-Al stack modelling was used for the material properties and the damage modelling adopted a user-defined as the Hashin's criteria in the fiber and the Puck criteria in the matrix. To define the delamination modelling in the interface cohesive, the contact algorithm applied for the ABAQUS/explicit.

5. ANALYSIS OF PHYSICAL MODEL AND FINITE ELEMENT MODEL

In this chapter, analysis of the results of the physical model and the FE model is introduced. In the CFRP-metal stack drilling process, the reason for internal defects is the critical thrust force. Therefore, thrust force prediction is more important for internal defect prevention. The effect of the spindle speed on the internal defect is found to be small. Therefore, the thrust force due to various feed rates for the same spindle speed is predicted. The results of the prediction of thrust force through two models are introduced and analyzed. In addition, the characteristics of each model are analyzed through comparison of the physical model and the FE model.

5.1 Physical model analysis

We estimated the thrust forces according to the total 6 stages. When machining the initial CFRP, the thrust force increased sharply and had a constant thrust force at full engagement stage. The thrust force is increased rapidly during aluminum machining and gradually decreased after the constant process. The thrust forces for various feeds are predicted at the same spindle speed 6000 rpm, and the critical thrust forces at the CFRP part and the aluminum part can be seen in figure 5.2.

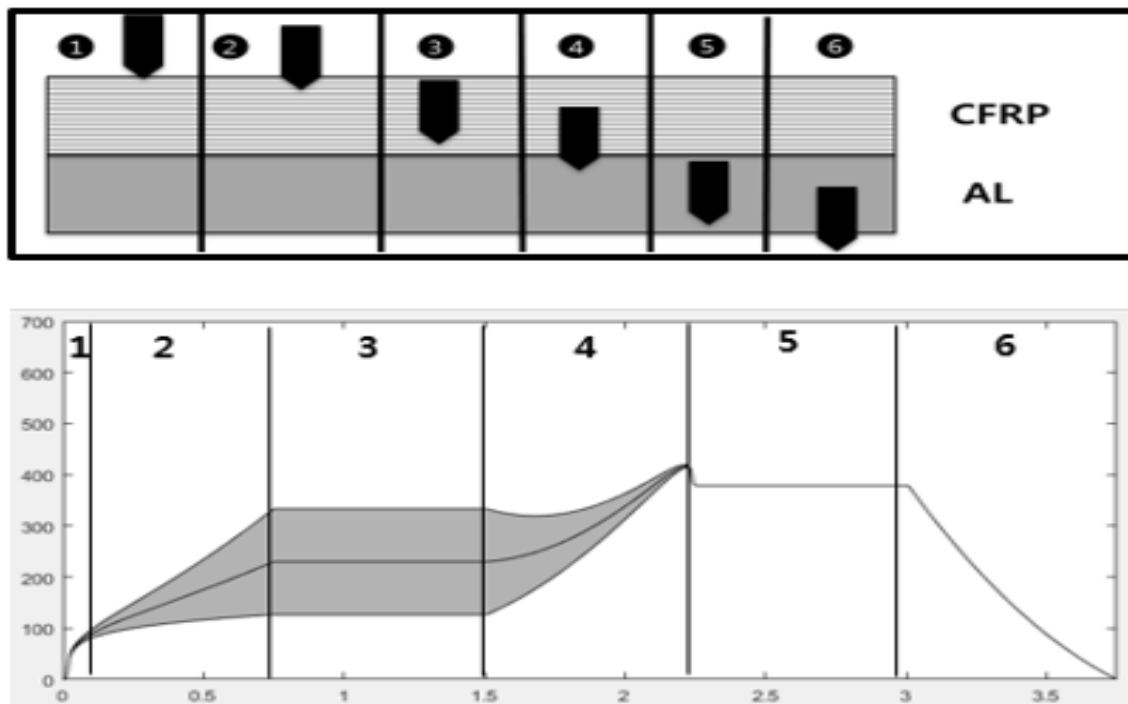


Fig. 5-1. Result of the physical model

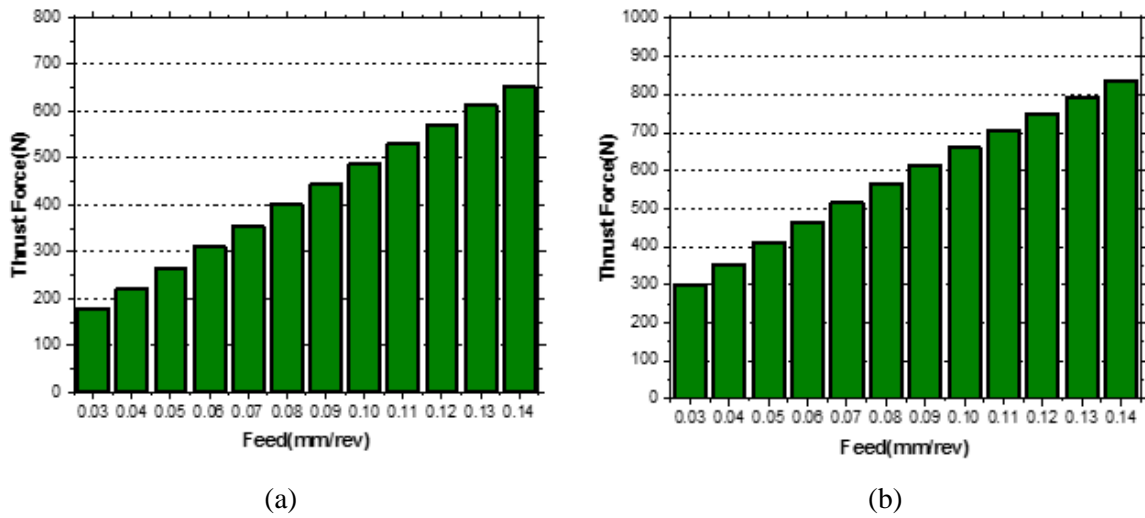


Fig. 5-2. Critical thrust force in (a) CFRP part, (b) aluminum part

The thrust force at the aluminum part was predicted to be higher than the thrust force at the CFRP part under all conditions. The critical thrust force also increased as the feed increased. The higher the feed, the better the processability. However, accurate thrust force prediction is needed because the processability is lowered when the thrust force over critical thrust force causing internal defect is applied to the material.

5.2 FE model analysis

The cutting force measurement in the drilling process is very important for the efficiency of the drilling process. Among them, the critical thrust force measurement is most important for the occurrence of delamination. The FE model can predict the thrust force that occurs during machining. We can predict the thrust force according to the drill position to determine the delamination as shown in figure 5-3. At the beginning of the graph, when the drill bit hit the CFRP plane, the thrust force increased and increased to the critical thrust force when it reached the aluminum plane. When drilling aluminum plane, the tool lip region is still drilling CFRP. For this reason, it is important to predict the critical thrust force according to the drill position. Critical thrust force was taken in the aluminum plane and then gradually decreased to zero.

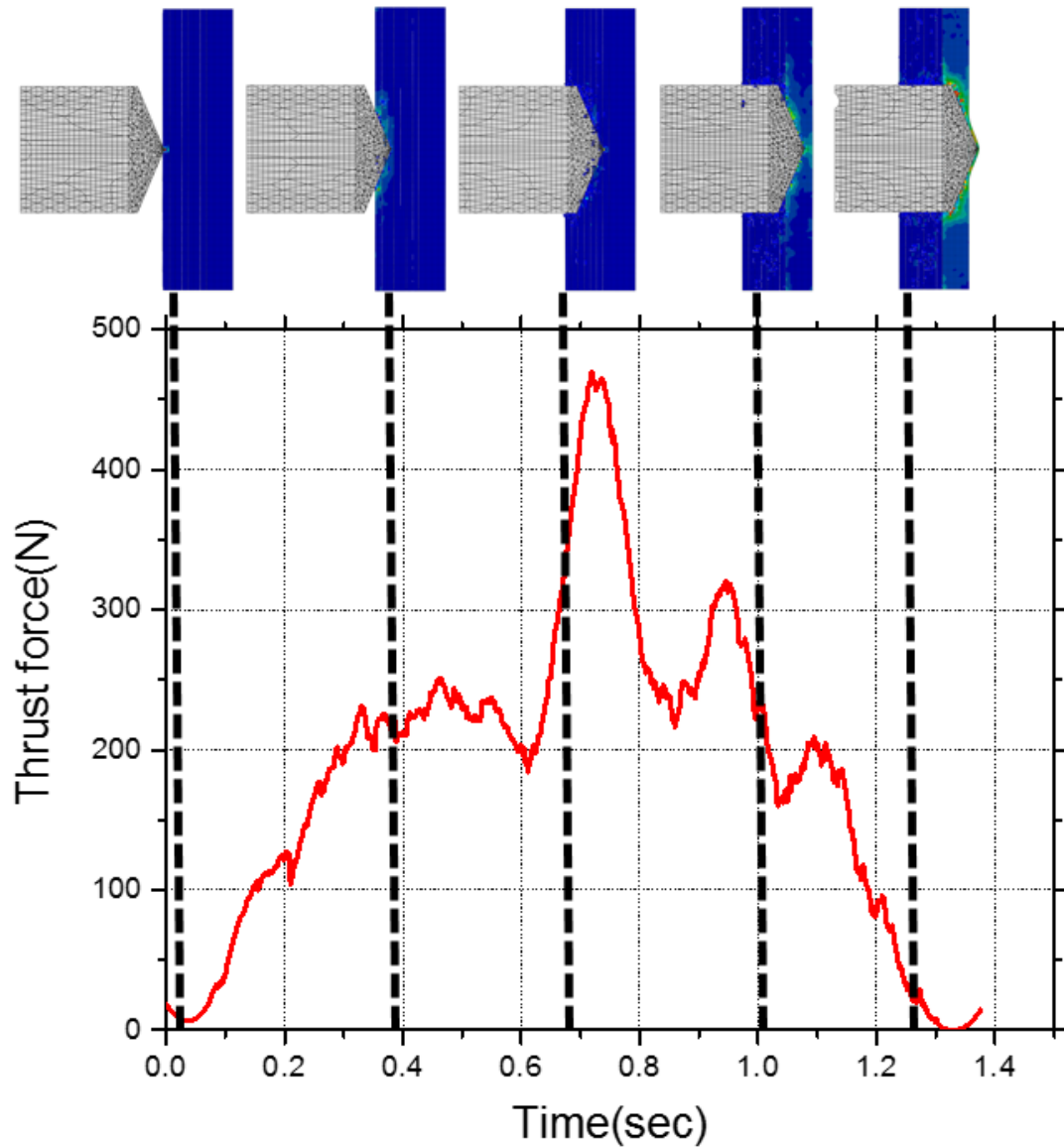


Fig. 5-3. Results of thrust force according to drill position

As the drill begins to process the CFRP, the thrust force begins to increase and shows a constant thrust force at full engagement with the CFRP. As starting to process aluminum, the thrust force increased to the maximum thrust force and the thrust force gradually decreased.

The FE model was used to calculate the thrust force under various conditions. The critical thrust force, which is the major cause of delamination, is shown by the CFRP part and aluminum part according to each condition which is shown in the figure 5-4.

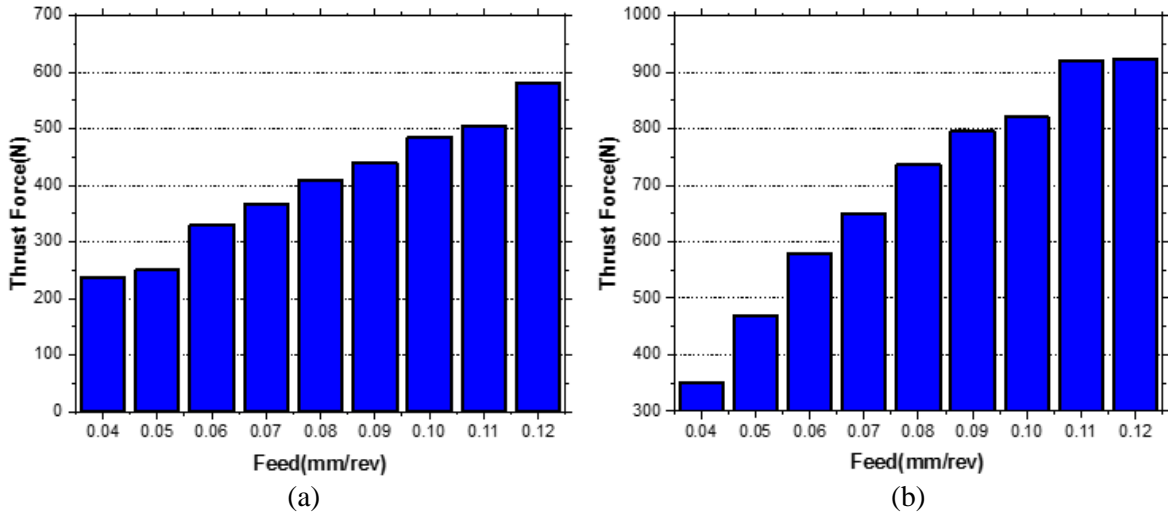


Fig. 5-4. Critical thrust force in (a) CFRP part, (b) aluminum part

The figure 5-4 shows that the critical thrust forces at the CFRP part and the aluminum part for various feeds at 6000 rpm. In the aluminum part, the thrust force is larger than that of the CFRP part, and the critical thrust force increases as the feed are increased for both the CFRP part and the aluminum part. In the CFRP-Al stack drilling process, high feed improves machining quality. However, as the feed rate increases with the increase of thrust force and simultaneously internal defects occur. Therefore, it is necessary to find proper machining conditions without internal defects through thrust force prediction.

It is important to predict the thrust force to predict delamination. The FE model not only predicts the thrust force but also shows the stress contour of the workpiece during drilling the stress contour has been shown in the figure. For these predictions, we can acknowledge where the location of the delamination occurrence and visually identify the forces received by the workpiece during CFRP-Al stack drilling. Figure 5-6 shows that the stress contour in the 7 layers of CFRP and aluminum in the drilling process. The drilling process is occurred with 6000rpm and feed 0.05mm/rev.

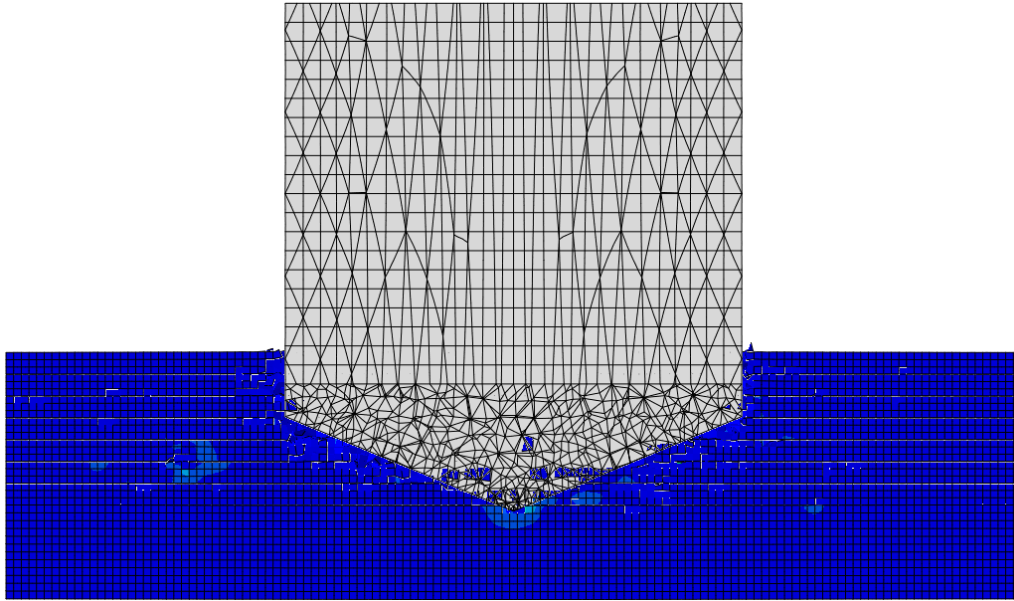


Fig. 5-5. CFRP-Al drilling simulation in FEM

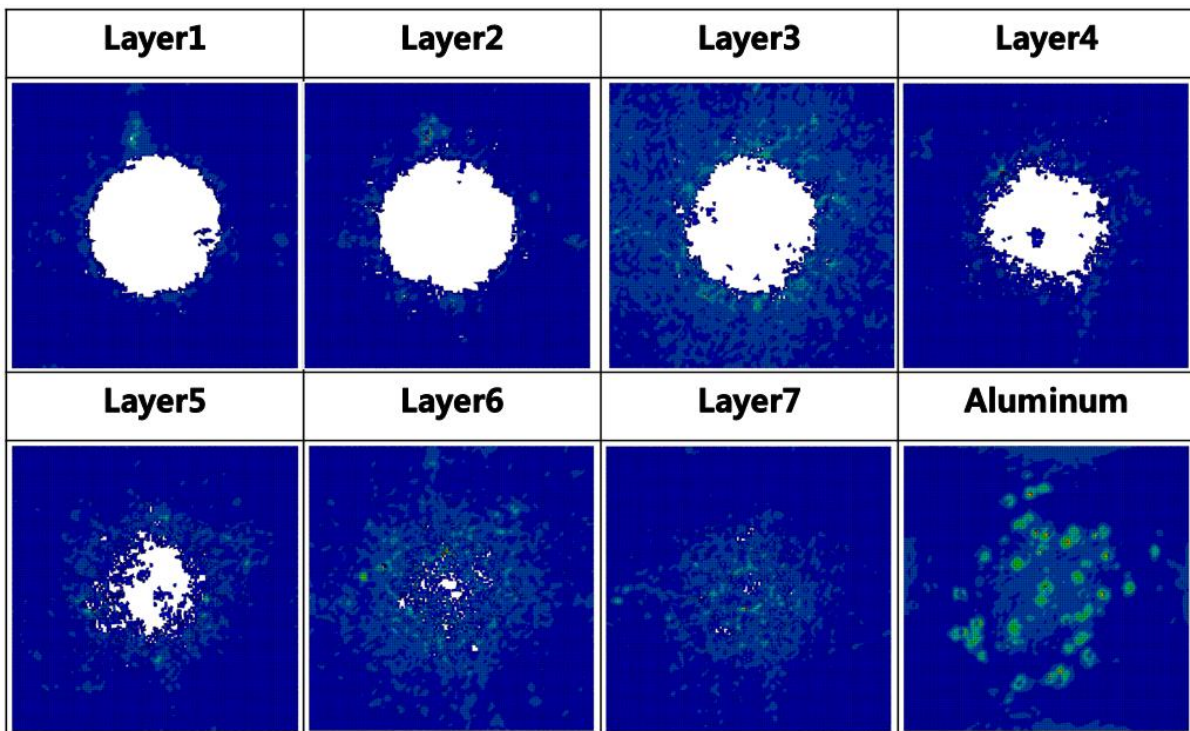


Fig. 5-6. Stress contour of FE model

The FE model has been used to identify the internal defects in real time. The overall defect after CFRP-Al stack drilling simulation can be seen in figure 5-7. CFRP internal defects are shown in each layer, and the degree of defects in each layer can be known through the deleted elements.



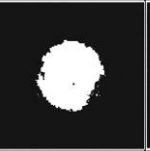
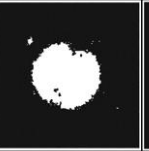
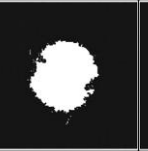
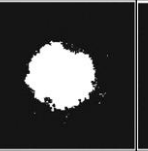
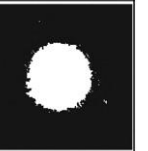


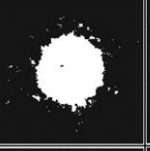
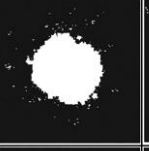
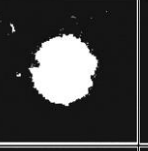
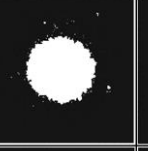


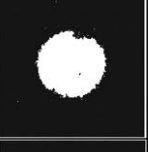


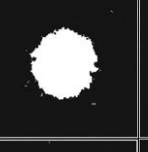



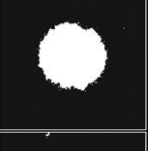



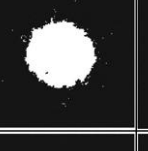

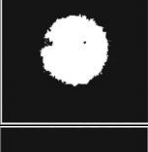








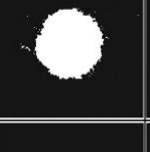




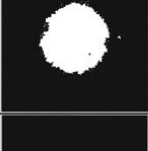
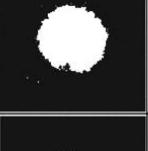
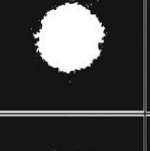




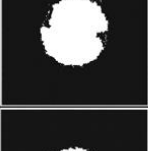
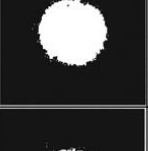









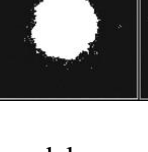


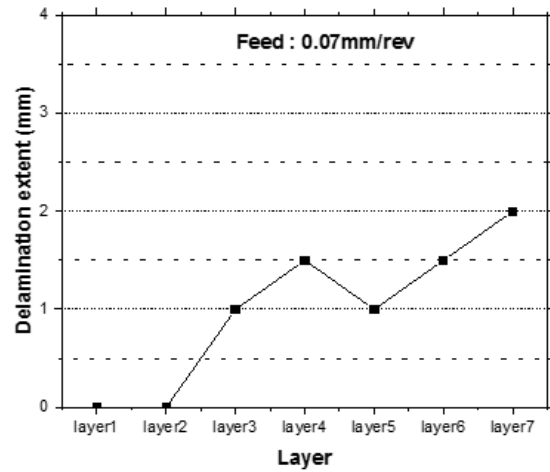
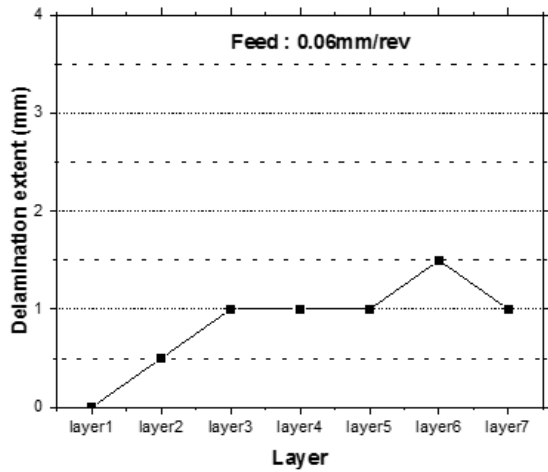
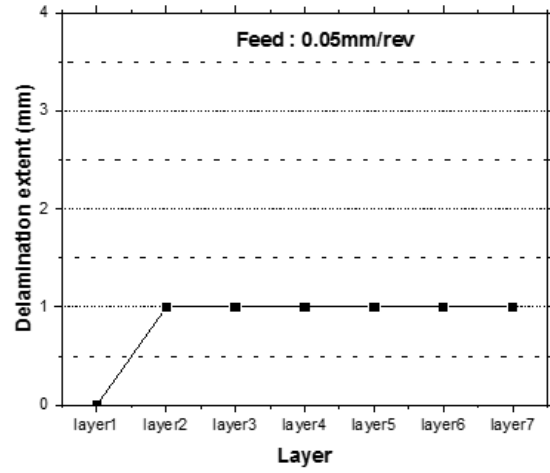
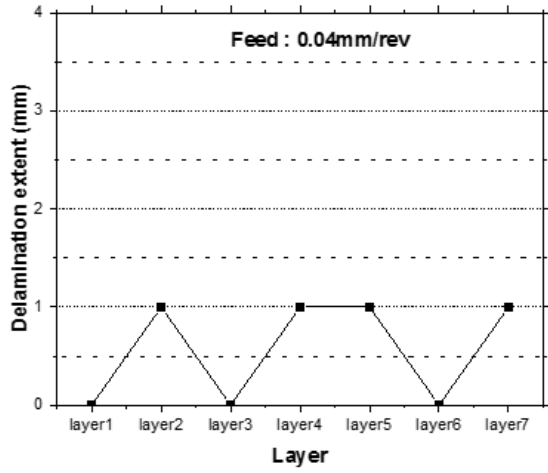
6000RPM	Layer1	Layer2	Layer3	Layer4	Layer5	Layer6	Layer7
0.04 mm/rev							
0.05 mm/rev							
0.06 mm/rev							
0.07 mm/rev							
0.08 mm/rev							
0.09 mm/rev							
0.10 mm/rev							
0.11 mm/rev							
0.12 mm/rev							

Fig. 5-7. Delamination in the FE model

Because of the FE model, delamination in each layer was measured. To measure the delamination, the distance to the deleted element was measured in each CFRP layer. The delamination extent is measured in this work according to the equation (5-1).

$$D_{ext} = D_{max} - D_{nom} \quad (5-1)$$



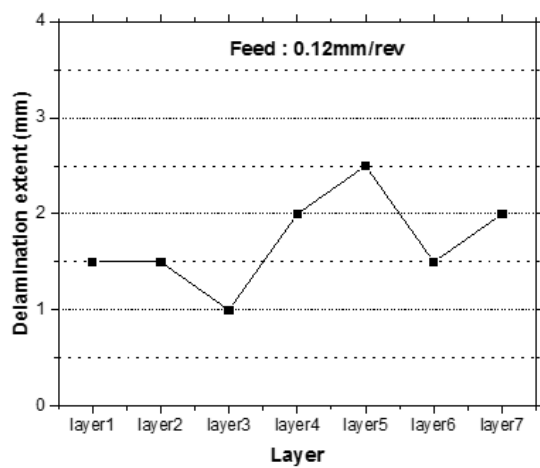
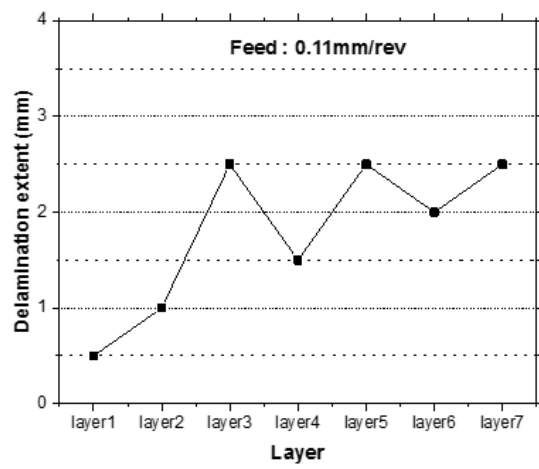
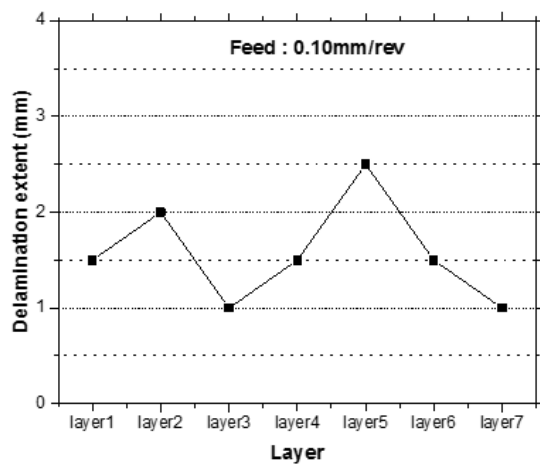
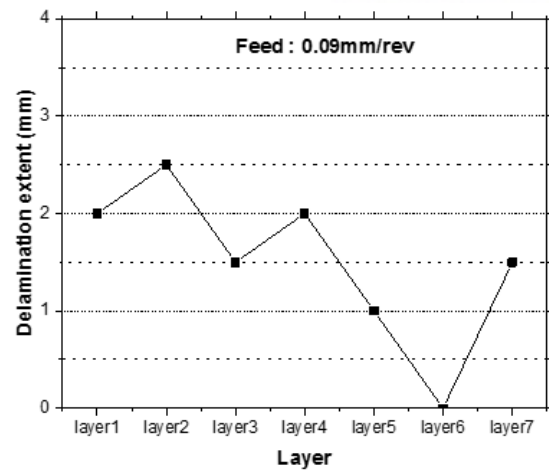
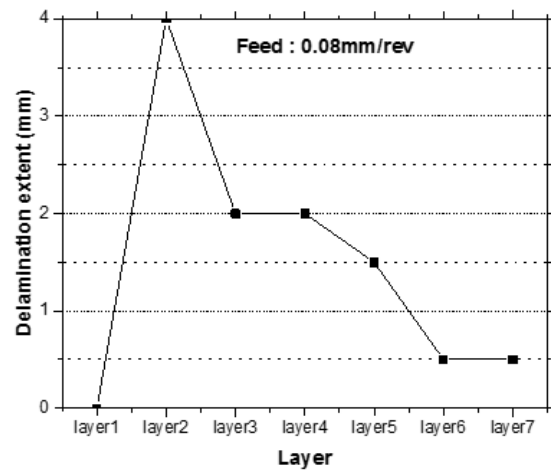


Fig. 5-8. Measurement of delamination extent

Fig. 5-8 shows that the extent of delamination. Overall, as the feed increases, the delamination extent increases. It can be seen clearly that the delamination extent increases from 0.08mm/rev. As the feed increases, the critical thrust force increases, resulting in increased delamination extent. No clear trends were observed when the layer was changed from 1 to 7 layers.

5.3 Comparison and analysis between the physical model and FE model

To compare the two models presented in this paper, the critical thrust forces predicted in each model are compared as shown in the figure 5-9. Comparing the CFRP part, the thrust force increases as the feed increases in both models. Overall, the critical thrust force in the physical model was predicted to be higher than the FE model. Similarly, in the aluminum part, the critical thrust force is increased for both models as the feed increases. Unlike the CFRP part, the predicted critical thrust force in the FE model of the aluminum part is larger than that of the physical model. This is the result of increasing the mesh size of the aluminum part to minimize the analysis time in the FE model. It is necessary to improve the accuracy of the model by comparing and verifying the experimental results with the predicted results of the two models.

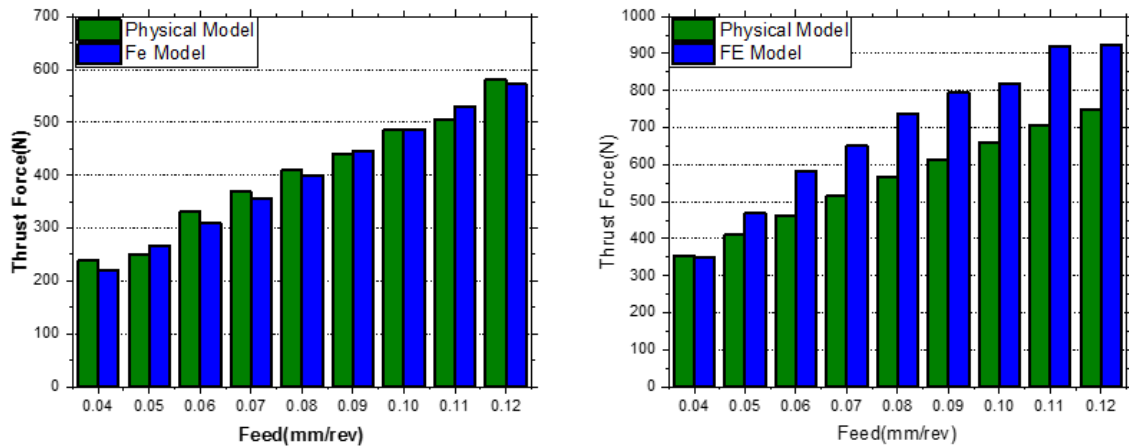


Fig. 5-9. Comparison of the critical thrust force between the physical model and FE model

5.4 Summary

In this chapter, the physical model and FE model results were analyzed. The predicted thrust forces in the physical model are divided by the CFRP part and the aluminum part. The critical thrust forces predicted under the respective conditions are represented for the both CFRP and aluminum which is an increase in the thrust force with increasing feed. In same as the physical model, the thrust force increases as the feed increases. FE model is very useful for the prediction of thrust forces and internal defects. The CFRP internal defects were confirmed by the prediction results according to the respective conditions, and the delamination extent was increased when the feed 0.8 mm / rev or more. The critical thrust forces of the FE model and physical model were similar in the CFRP part, but in the aluminum part, the predicted thrust force was larger in the FE model.

6. EXPERIMENTAL VALIDATION

6.1 Experimental setup

The experiment has been done by 5-axis CNC machine and performed the CFRP-Al stack drilling operation. A dynamometer (KISLER 9257B type) has been used for measuring the thrust force in the drilling experiment. The tool has a Kennametal B221A (Solid Carbide drill) with a diameter of 9mm, a helix angle of 30° and a point angle of 135°. The experiment setup is shown in figure 6-1. To compare the thrust force and delamination according to the feed (mm / rev), the experiment has been carried out in 72 different conditions with 12 different feeds and 6 spindle speeds. The experimental conditions of CFRP-Al stack drilling process are shown in figure 6-2.

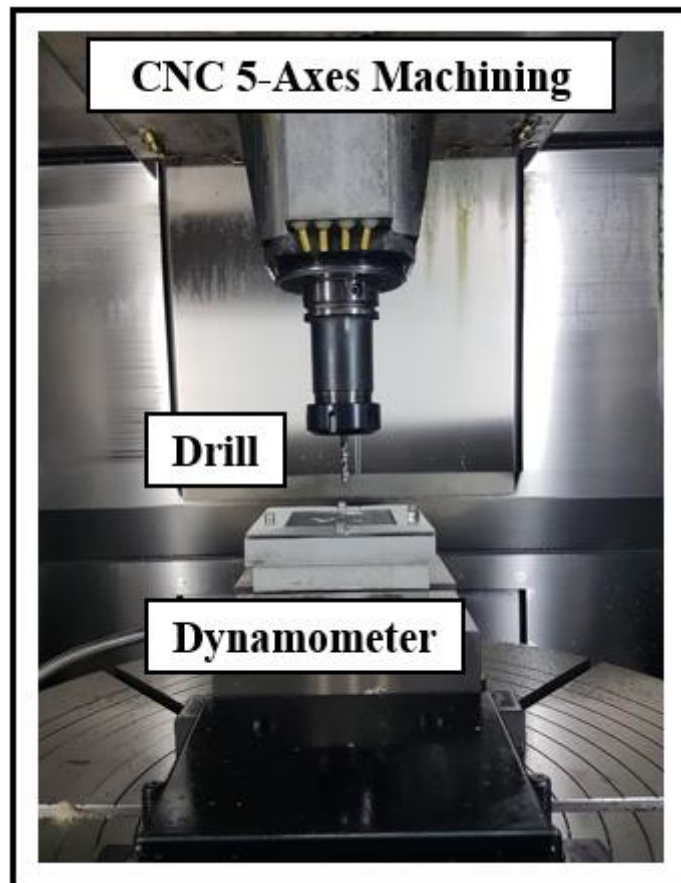


Fig. 6-1 Experimental set for CFRP-Al stack drilling

Cutting speed	500rpm	1000rpm	2000rpm	4000rpm	6000rpm	8000rpm
Feed [mm/rev]	0.03	0.03	0.03	0.03	0.03	0.03
	0.04	0.04	0.04	0.04	0.04	0.04
	0.05	0.05	0.05	0.05	0.05	0.05
	0.06	0.06	0.06	0.06	0.06	0.06
	0.07	0.07	0.07	0.07	0.07	0.07
	0.08	0.08	0.08	0.08	0.08	0.08
	0.09	0.09	0.09	0.09	0.09	0.09
	0.10	0.10	0.10	0.10	0.10	0.10
	0.11	0.11	0.11	0.11	0.11	0.11
	0.12	0.12	0.12	0.12	0.12	0.12
	0.13	0.13	0.13	0.13	0.13	0.13
	0.14	0.14	0.14	0.14	0.14	0.14

Fig. 6-2. Experimental conditions of CFRP-Al drilling process

A stack of 3mm high multi-direction carbon fiber reinforced plastics and 2 mm high Al-6061 alloy were used, and the size of the CFRP-Al stack 100×100 mm as shown in figure 6-3. This multi-directional CFRP is stacked in $0^\circ/90^\circ$ and carbon plain with an epoxy resin matrix. In addition, a customized jig has been fabricated to fix the CFRP-Al stack in the experiment as shown in figure 6-4.

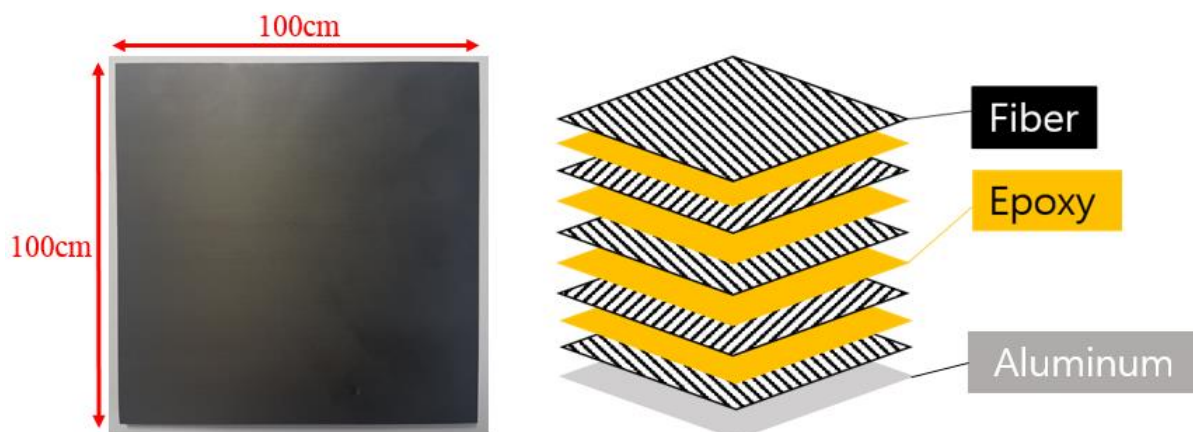
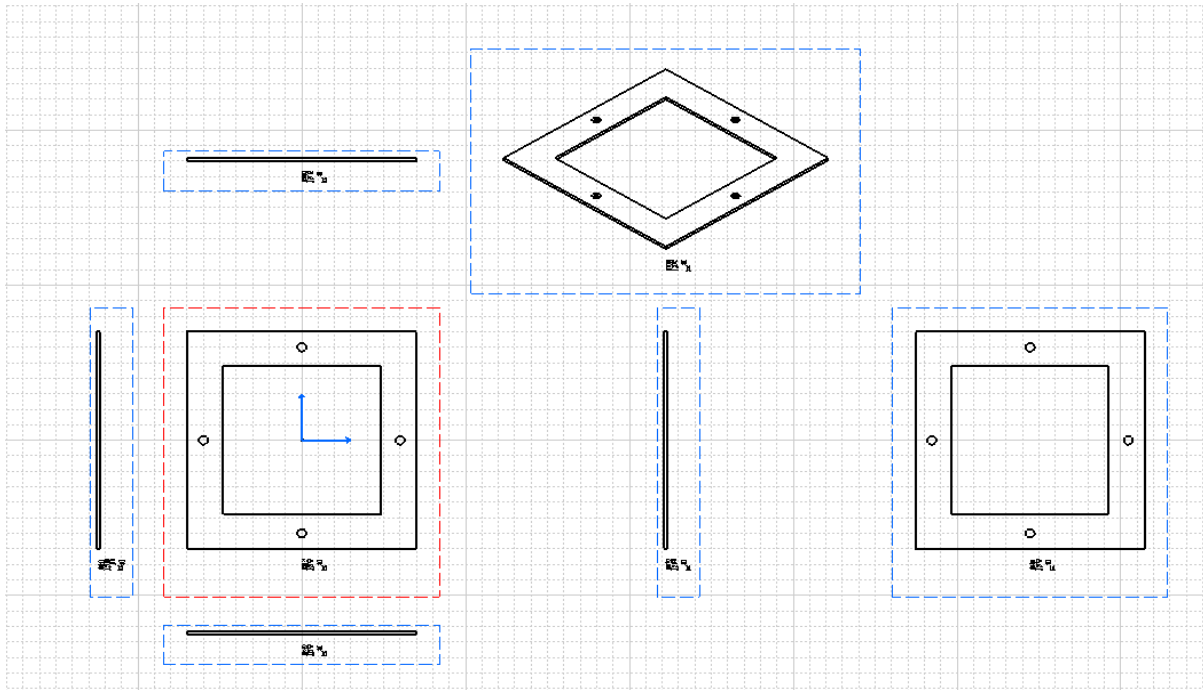
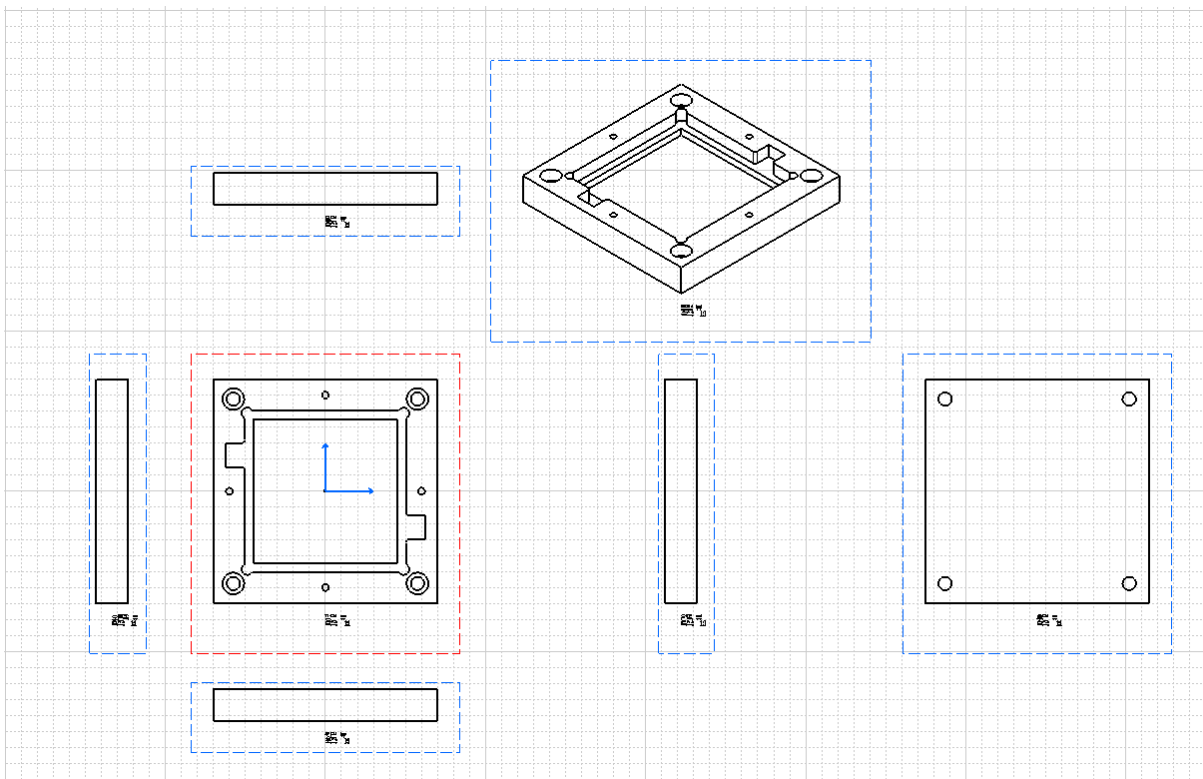


Fig. 6-3. The CFRP-Al stack



(a)



(b)

Fig. 6-4 Design of the jig system (a) Top jig (b) Bottom jig

6.2 Experimental results

The results of the CFRP-Al stack drilling test under 72 conditions are shown in figure 6-5. 36 drilling processes were performed on a CFRP-Al stack of 100×100 . The thrust force was measured with the use of a tool dynamometer, and a CT image was taken to identify internal defects.

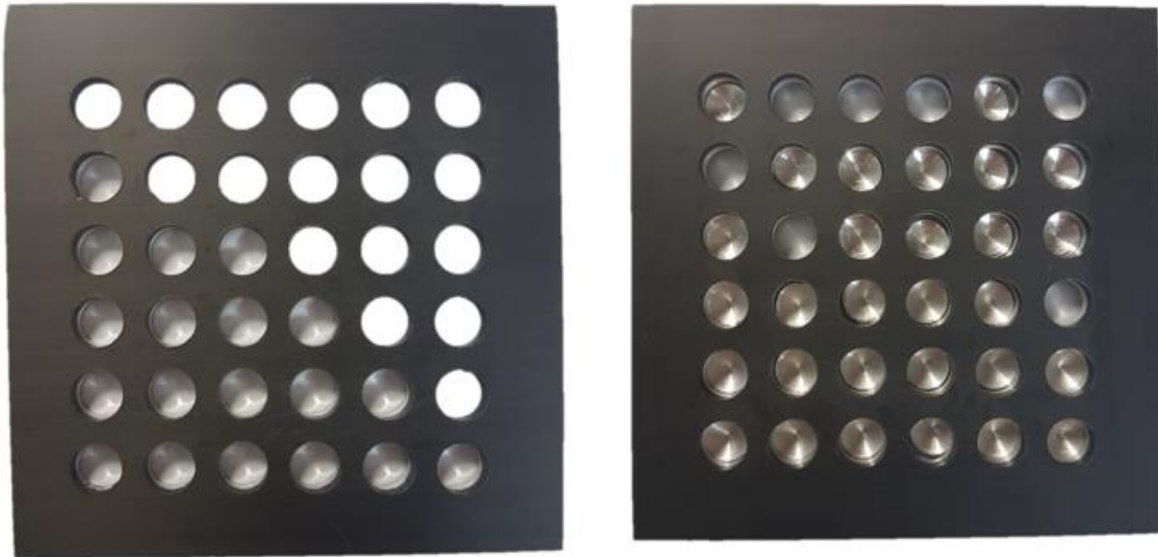


Fig. 6-5. CFRP-Al stack drilling experiment result

6.2.1 Thrust force

In this section, thrust force obtained from the experiment was analyzed. The material used in the drilling process is a stack of CFRP of 0° and 90° and Al-6061 alloy. After CFRP molding, the structure was bonded with aluminum. The carbon fiber used was MRC TR50 and SKR-K51 was used for the resin. The drilling conditions were 6 kinds of RPM (500rpm, 1000rpm, 2000rpm, 4000rpm, 6000rpm, 8000rpm) and 12 kinds of cutting speeds (0.03mm / rev, 0.04mm / rev, 0.05mm / rev, 0.06mm / rev, 0.13 mm / rev, 0.14 mm / rev). The thrust forces according to the same feed are compared. The results of the thrust force according to each experimental condition were examined (Fig. 6-6).

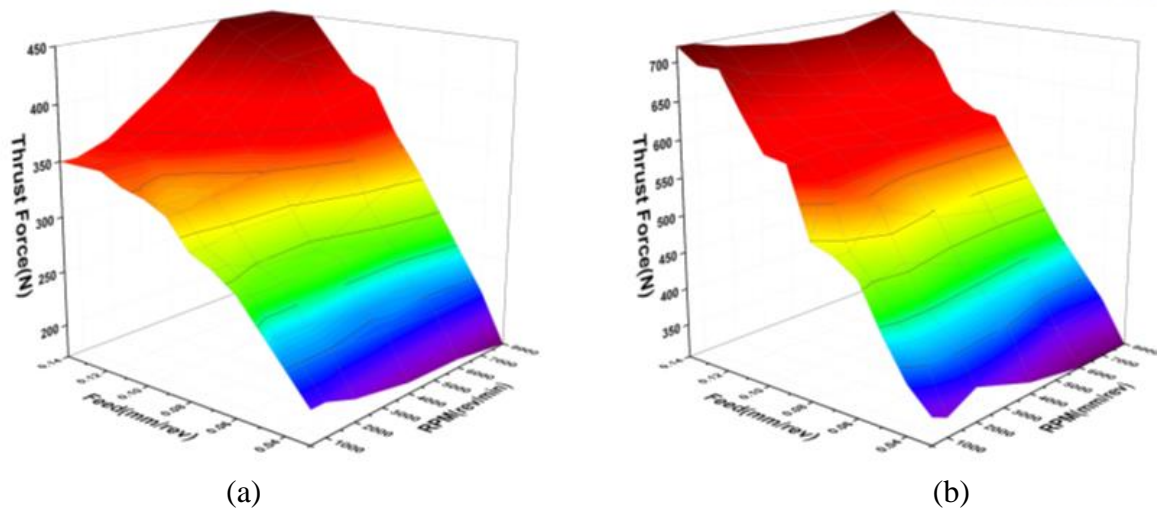


Fig 6-6. Thrust force results according to each machining condition (a) CFRP part (b) aluminum part

Overall, according to the figure 6-6 the thrust force increases as the feed increases. At the same feed value, the thrust force values according to RPM show the same overall though there are some errors in the CFRP part. There is almost no change in thrust force due to RPM, and the thrust force change due to the feed is large. Therefore, the main problem in the CFRP-Al stack drilling process is the thrust force, which is the main cause of the delamination, so the problem must be solved by focusing on the feed condition rather than the RPM condition.

6.2.2 Delamination

Whether delamination occurs in the CFRP-Al stack drilling process is very important. The biggest problem of the CFRP-Al stack drilling process is delamination of CFRP. As the quality of the machining is determined by the occurrence of delamination. The experiment was performed to measure delamination. As a result of the experiment, the surface delamination was measured according to each condition. The degree of surface delamination was visually distinguishable, and delamination was determined through the delamination extent. The following figure shows the result of measuring the delamination extent according to each condition.

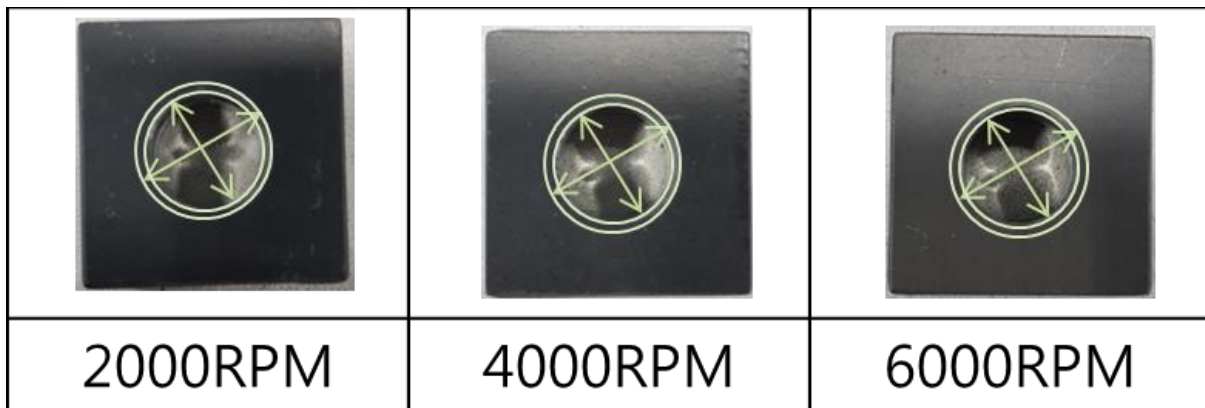


Fig. 6-7. Delamination extent according to RPM in the same feed



Fig. 6-8. Delamination extent according to feed in the same RPM

As shown in figure 6-7 and 6-8, the delamination extent shows the same trend in the same feed value. Surface delamination is almost the same as the RPM change according to the same feed. On the other hand, it shows that the delamination extent increases as the feed increases in the same RPM. Therefore delamination is more related to the feed rate than to the cutting rate, which is related to an increase in the thrust force as the feed increases. As the feed increased, the thrust force increased, and internal defects increased.

As the quality of the machining is determined by the occurrence of delamination, a model for predicting the delamination in CFRP-Al stack drilling machining is needed. In this paper, the developed FE model for predicting delamination discrimination in CFRP-Al stack drilling process is introduced. Experimental DB-based delamination discrimination has been performed, and the degree of delamination was analyzed which shown in figure 6-9.

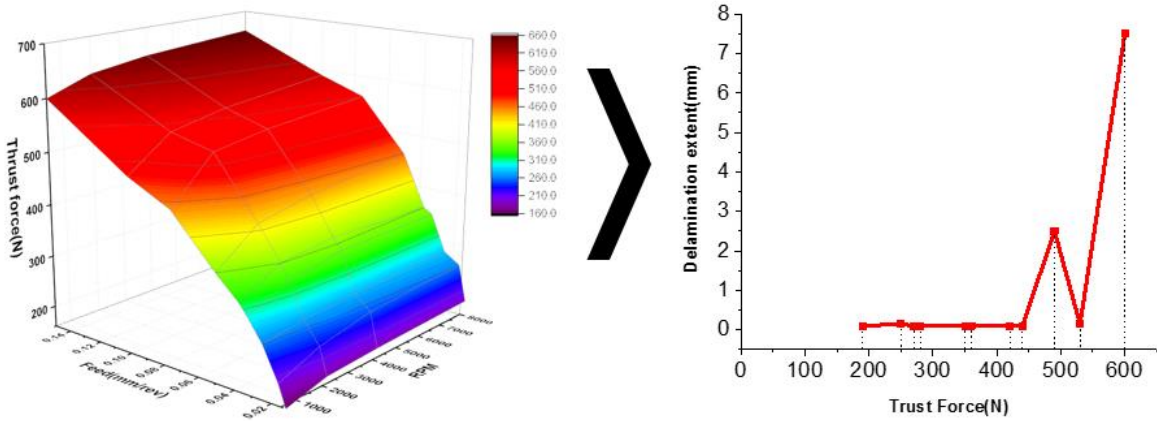


Fig. 6-9. Experimental based delamination discrimination

Unlike the surface delamination, the internal defect cannot be visually confirmed. Therefore, a CT scan was performed to examine the defect inside the CFRP-Al stack as shown in figure 6-10. The overall internal delamination was confirmed by CT scan and compared with the FE model.

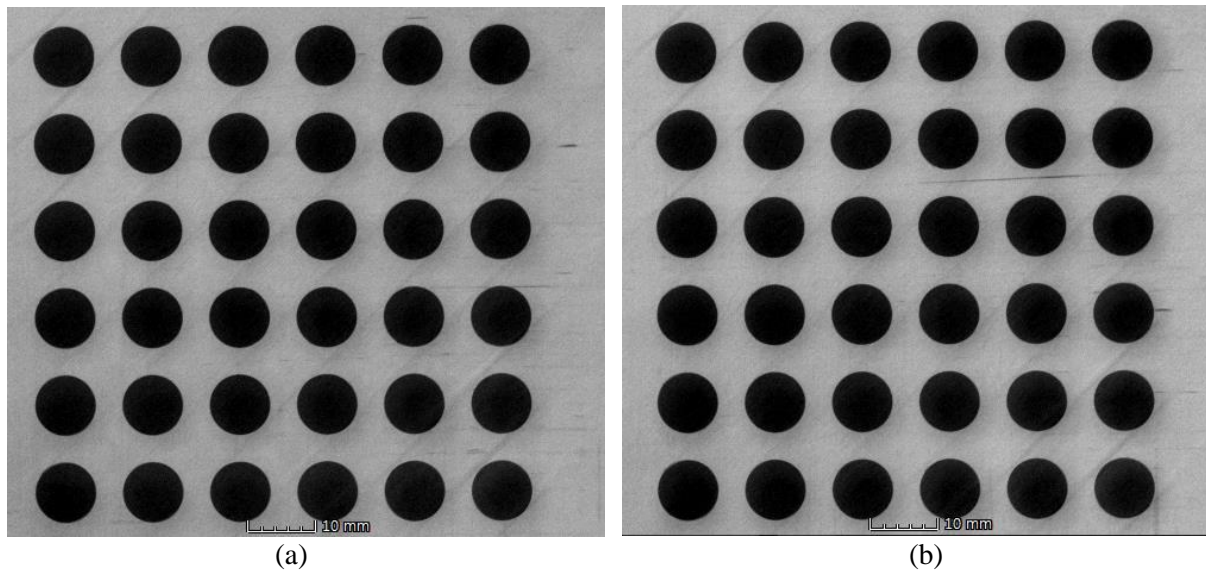


Fig. 6-10. CFRP-Al stack internal defect (a) 1.42mm, (b) 0.91mm

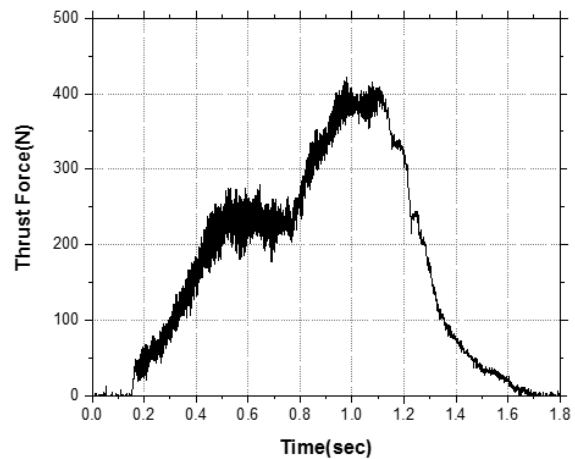
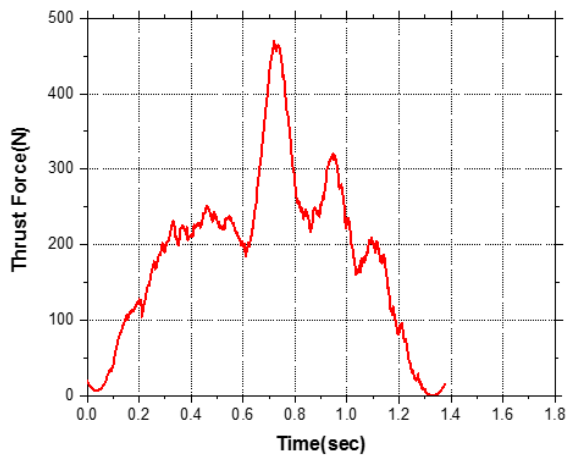
Internal defects were observed by CT scan. Internal defects of all heights were observed with respect to the drilling axis, and the inside of the side was also observable. Because of the internal defect analysis, it was found that the delamination extent increases as the internal feed also increases. Also, as RPM increased, there was almost no difference in the delamination extent.

6.3 Numerical model validation

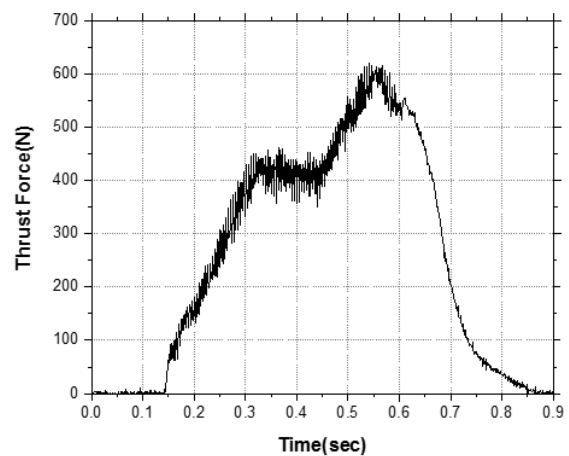
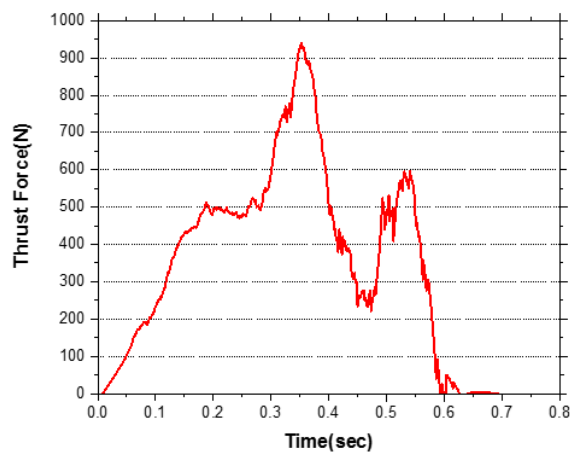
In this section, the experimental results of CFRP-Al stack drilling process and the predicted results in the two models are compared and verified. Through the comparison and verification, the importance of predictive model will be shown by reliability verification of two models.

6.3.1 Thrust force validation

To compare the experimental results with the prediction model, the thrust force values at various feed conditions for the same RPM were predicted through prediction model. Since the thrust force results in the same feed are almost identical, we assumed that the thrust forces in the same feed are the same in this paper.



(a)



(b)

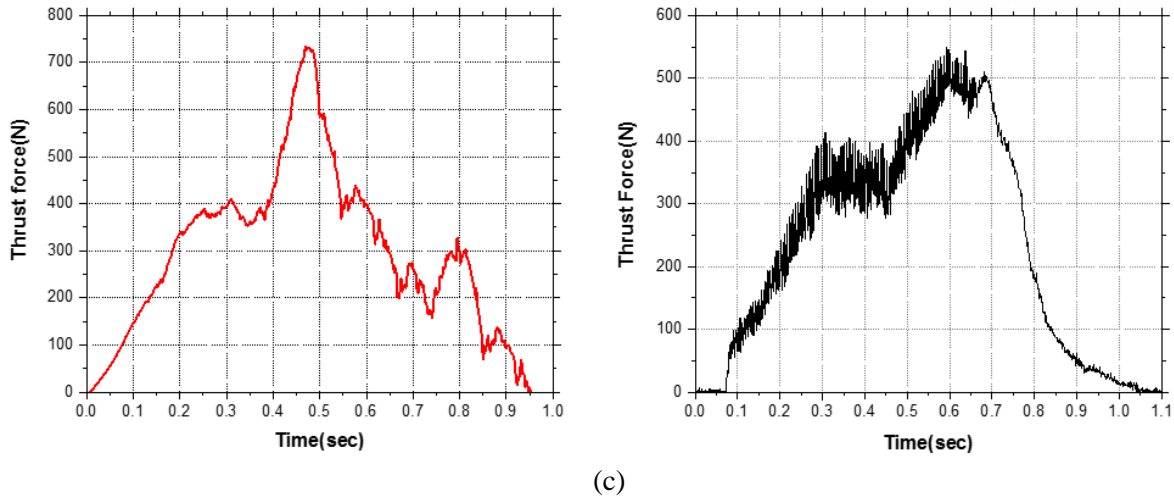


Fig. 6-11. Comparison of Thrust Force between Simulation and Experimental Results

(a) 6000rpm, 0.05mm/rev, (b) 6000rpm, 0.08mm/rev, (c) 6000rpm, 0.11mm/rev

Both predicted models predicts the thrust forces at various feed conditions for the same RPM since we found that there was very little thrust force variation for the same RPM by reference and experimental results. The predicted thrust force in each model is shown in figure 6-12 by calculating critical thrust force in CFRP part and the aluminum part.

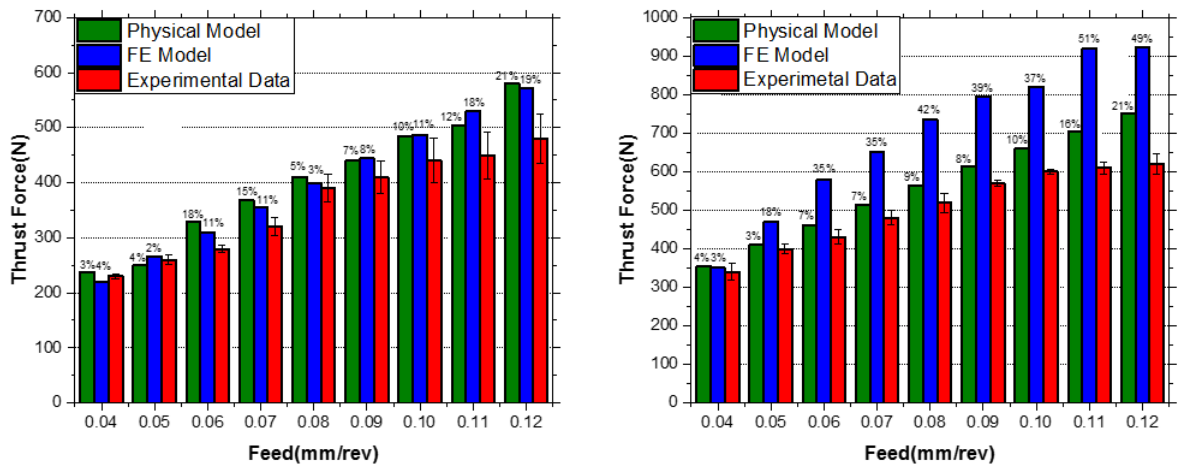








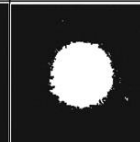
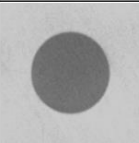
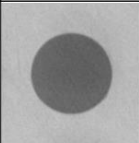
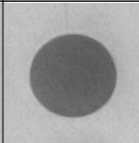
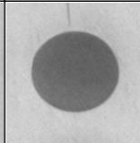
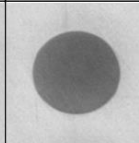
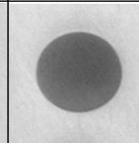
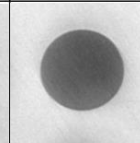
Fig. 6-12. Comparison of critical thrust force results of two models and experiments



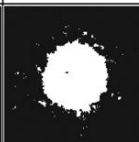
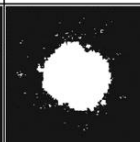
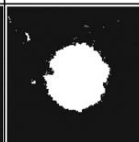

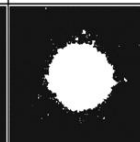

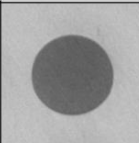
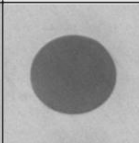
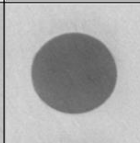
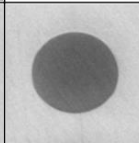
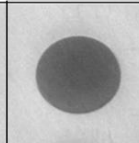
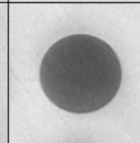
As a result of comparing the experimental results with two numerical models, it can be seen that the error rate increases with the increase of feed in both CFRP part and the aluminum part. Experimental results show that the error range increases as the feed increases, because of the thrust force changes due to vibration and various causes as the feed rate increases.







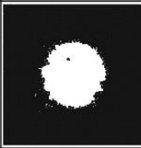
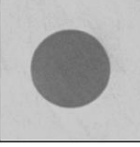
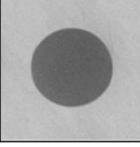
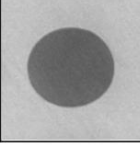
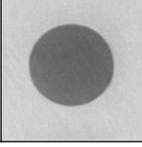
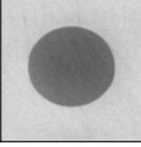
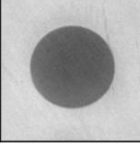
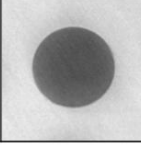
Comparing the physical model results with the experimental results, the error rate is within 21% for the CFRP part and within 20% for the aluminum part. As the feed increases, the thrust force increases, and the critical thrust force increases in the aluminum part compared to the CFRP part. Comparing the FE model results with the experimental results, the error rate of the CFRP part was similar to that of the physical model within 21%, but the error rate was up to 50% in the aluminum part. Because the mesh size in the aluminum part is larger than the CFRP part to shorten the CFRP-Al stack drilling process simulation time. In the FE model, the critical thrust force increases as the feed increases.

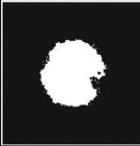
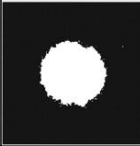
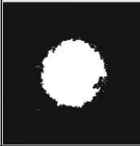
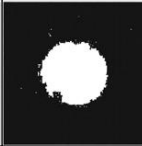
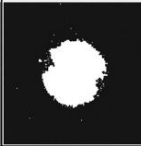

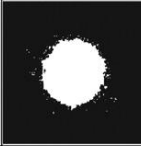
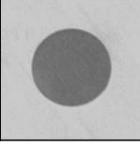
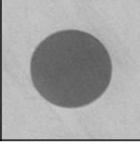
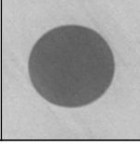
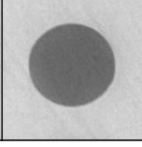
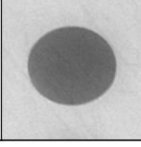
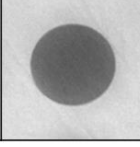
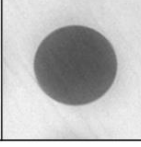
6.3.2 Delamination validation

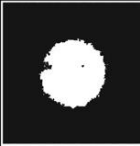



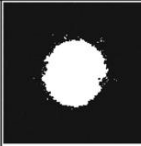


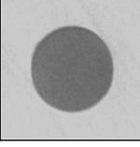
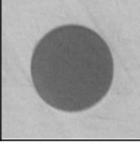
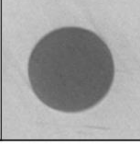
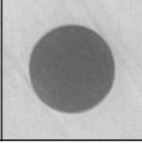
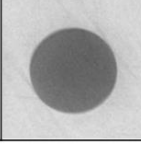
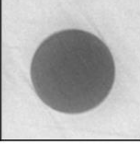
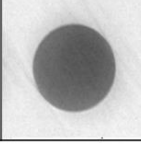
Based on the experimental results, it was compared with the internal delamination predicted from the FE model. Experimental results show that delamination is more affected by feed than RPM, so we predict delamination in various feeds according to the same 6000 rpm in simulation as shown in figure 6-13.







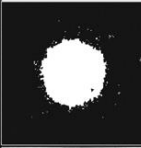
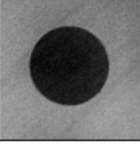
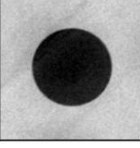
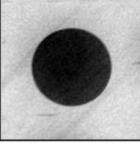
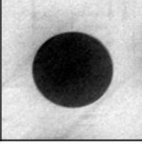
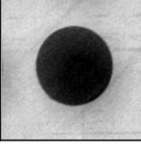
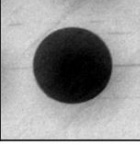
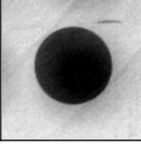
0.04mm/rev	Layer1	Layer2	Layer3	Layer4	Layer5	Layer6	Layer7
FE Model							
Experiment							




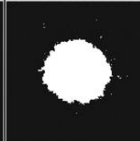
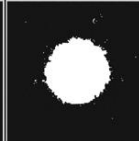
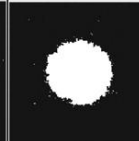
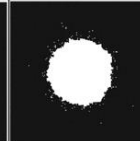
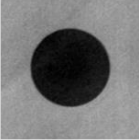
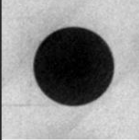
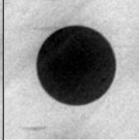
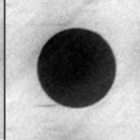
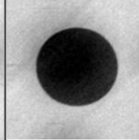
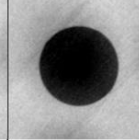
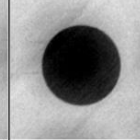
0.05mm/rev	Layer1	Layer2	Layer3	Layer4	Layer5	Layer6	Layer7
FE Model							
Experiment							




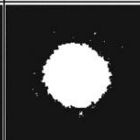
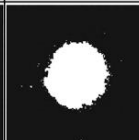
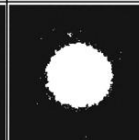
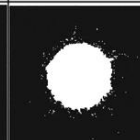
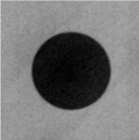
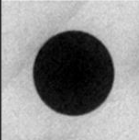
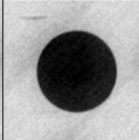
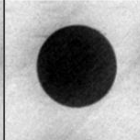
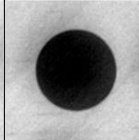
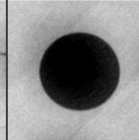
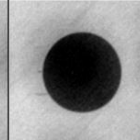
0.06mm/rev	Layer1	Layer2	Layer3	Layer4	Layer5	Layer6	Layer7
FE Model							
Experiment							

0.07mm/rev	Layer1	Layer2	Layer3	Layer4	Layer5	Layer6	Layer7
FE Model							
Experiment							

0.08mm/rev	Layer1	Layer2	Layer3	Layer4	Layer5	Layer6	Layer7
FE Model							
Experiment							

0.09mm/rev	Layer1	Layer2	Layer3	Layer4	Layer5	Layer6	Layer7
FE Model							
Experiment							

0.10mm/rev	Layer1	Layer2	Layer3	Layer4	Layer5	Layer6	Layer7
FE Model							
Experiment							

0.11mm/rev	Layer1	Layer2	Layer3	Layer4	Layer5	Layer6	Layer7
FE Model							
Experiment							






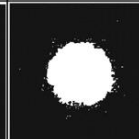
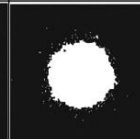
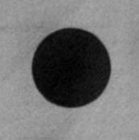
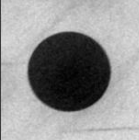
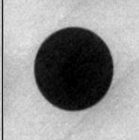
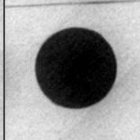
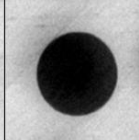
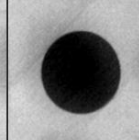
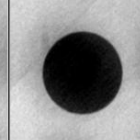
0.12mm/rev	Layer1	Layer2	Layer3	Layer4	Layer5	Layer6	Layer7
FE Model							
Experiment							

Fig. 6-13. Comparison of delamination between experimental and prediction model

Comparison of experiment and numerical model, it shows good machinability when the feed was under the 0.8mm/rev. When the feed was 0.8 mm / rev or more, it showed delamination in CFRP-Al stack drilling process. FE model simulation results and CT image comparison results showed almost similar trends but there was no regular trend of delamination occurrence by layer. Based on these results, the measured delamination in each feed was compared as shown in Figure 6-14.

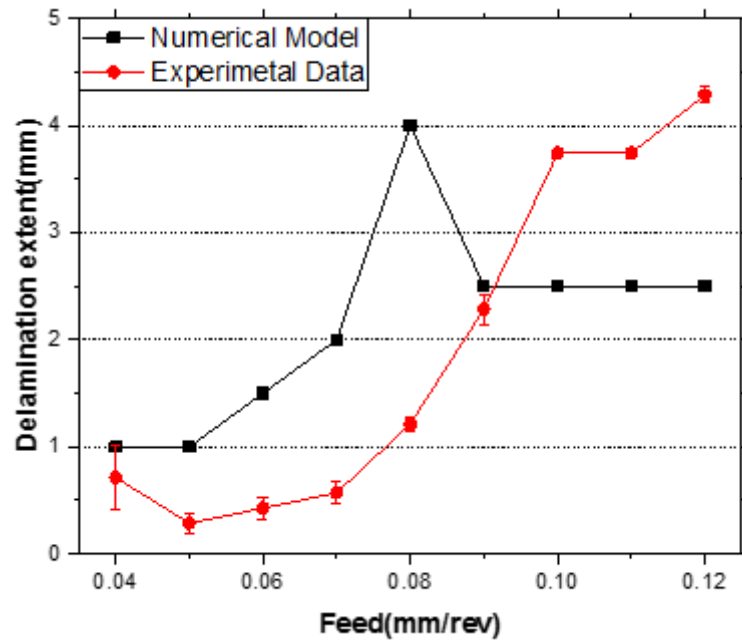


Fig. 6-14. Variation of delamination

6.4 Summary

In this chapter, the validity of the simulation is verified through comparison with the numerical model and experimental results. A physical model was created by applying the mechanism described in Chapter-3 and the thrust force was predicted according to drilling conditions. In the FE model using ABAQUS / Explicit software, thrust force and delamination prediction were performed by applying a damage model. In addition, stress contour was observed during drilling and stress was observed in real time. The reliability of the model was shown by comparing the experimental results with the numerical model. In the physical model, the error rate was within 21% for CFRP part and 21% for aluminum part. In the FE model, the CFRP part exhibited a maximum error of 50% in the aluminum part within 20%.

7. CONCLUSIONS AND FUTURE WORKS

7.1 Contributions and Conclusions

The purpose of this study is to develop a numerical model to predict thrust force and delamination in CFRP-Al stack drilling. Because CFRP demonstrates heterogeneous characteristics, CFRP machining is distinguished from metal cutting. The problem in CFRP machining is the delamination, and the major cause of delamination is the critical thrust force. To solve this problem, two numerical models have been developed.

The physical model based on Zhang's model predicts the thrust force and discriminates the delamination based on the experimental DB. A mechanism considering fiber orientation was used and a mechanism applicable to the 3D drilling process through a coordinate transformation in 2-dimensional orthogonal cutting was used. Thrust force predictions of 72 different conditions were obtained. As a result of comparison with the experimental results, the error rate was within 21% in the CFRP part and within 20% in the aluminum part. Delamination occurred when the critical thrust force exceeded 440N through the experimental DB.

FE model using ABAQUS / Explicit software is simply modeled to predict the thrust force and internal defects through optimal analysis time. Damage model with Hashin's criteria in the fiber failure and Puck criteria in the matrix failure delamination modelling was considered for the simulation using VUMAT. And cohesive zone was used to delamination modelling. Through the FE model, the thrust force values in various feeds with the same rpm were predicted. The error rate was within 21% of the CFRP part and within 50% in the aluminum part. The stress contour of each layer during the drilling process was confirmed and the contour of the critical thrust force was confirmed. Also, the delamination extent of each layer was determined, and the extent of delamination increased with increasing feed. When the feed was 0.08 mm/rev or more, the delamination extent was significantly increased, which was similar to the experimental results.

7.2 Future works

In this study, we suggested thrust force and delamination prediction model in CFRP-Al stack drilling. The delamination discrimination proposed in the physical model was based on an experimental basis. It is possible to develop the Jahromi [53] model, which proposes a damage prediction model in CFRP orthogonal cutting, by expanding it in three dimensions through the dimension transformation used in this prediction model. We predicted thrust force and delamination in the FE model using ABAQUS / Explicit software program. It can be concluded that the error rate can be reduced by considering the complex cross-section of the model because it does not coincide exactly with the experiment. It is also considered to be expandable to models considering heat. These developments enable the drilling of CFRP-Al stacks under optimal processing conditions. It can also develop a numerical model for the titanium stack drilling process.

REFERENCES

1. C. Soutis. Fibre reinforced composite in aircraft construction. *Prog Aerosp Sci*, 41 (2) (2005), pp. 143-151.
2. P. De Goeje and K. E. D. Wapenaar. Non-destructive inspection of carbon fibre - reinforced plastics using eddy current methods. *Composites*, 23(3) (1992), pp. 147-157.
3. A.M. Abrão, P.E. Faria, J.C.C. Rubio, P. Reis, J.P. Davim. Drilling of fiber reinforced plastics: a review *J Mater Process Technol*, 186 (1–3) (2007), pp. 1-7.
4. Statista, 2017, “Global demand for carbon fiber from 2010 to 2022”, <https://www.statista.com/statistics/380538/projection-demand-for-carbon-fiber-globally/>
5. J.Y. Xu, Q.L. An, X.J. Cai, M. Chen. Drilling machinability evaluation on new developed high-strength T800S/250F CFRP laminates. *Int J Precis Eng Manuf*, 14 (10) (2013), pp. 1687-1696.
6. Wong TL, Wu SM, Groy GM. An analysis of delamination in drilling of composite materials. In: *Proceedings of the 14th SAMPE technology conference*. Atlanta, GA, USA; (1982), pp. 471–483.
7. El-Sonbaty, U.A. Khashaba, T. Machaly. Factors affecting the machinability of GFR/epoxy composites. *Compos Struct*, 63 (2004), pp. 313-327.
8. H. Ho-Cheng, C.K.H. Dharan. Delamination during drilling of composite laminates. *J Eng Ind, ASME*, 112 (1990), pp. 236-239.
9. U.A. Khashaba Delamination in drilling GFR-thermoset composites. *Compos Struct*, 63 (2004), pp. 313-327.
10. R. Teti, V. Lopresto, A. Caggiano, High performance cutting of fibre reinforced plastic composite materials. *Procedia CIRP* 46 (2016), pp. 71-82

11. Meng, Q., Zhang, K., Cheng, H., Liu, S., & Jiang, S. An analytical method for predicting the fluctuation of thrust force during drilling of unidirectional carbon fiber reinforced plastics. *Journal of Composite Materials*, 49(6) (2015), pp. 699-711.
12. Qi, Z., Zhang, K., Cheng, H., Wang, D., & Meng, Q. Microscopic mechanism based force prediction in orthogonal cutting of unidirectional CFRP. *International Journal of Advanced Manufacturing Technology*, 79 (2015).
13. M.P. Groover. *Fundamental of modern manufacturing*. John Wiley & Sons, nc., New Jersey (1999) pp. 102–104.
14. Lopresto, V., Caggiano, A., & Teti, R.. High performance cutting of fibre reinforced plastic composite materials. *Procedia CIRP*, 46 (2016), pp. 71-82.
15. D. Arola, M. Ramulu, D.H. Wang. Chip formation in orthogonal trimming of graphite/epoxy composite Composites. *A27* (1996), pp. 121-133.
16. A. Koplev, Aa. Lystrup, and T. Vorm. The Cutting Process, Chips, and Cutting Forces in Machining CFRP. *Composites*, Vol. 14, No. 4 (1983), pp. 371-376.
17. Caggiano, A. Machining of fibre reinforced plastic composite materials. *Materials* (2018), 11, 442.
18. V. Krishnaraj, A. Prabukarthi, M. Senthilkumar, B. ArunRamanathan, N. Elangovan, R.Zitoune, J. Davim. Optimization of machining parameter at high speed drilling of carbon fiber reinforced plastic (CFRP) laminates *Composites: Part B*, 43 (2012), pp. 1791-1799.
19. Qi Z, Zhang K, Cheng H, Wang D, Meng Q. Microscopic mechanism based force prediction in orthogonal cutting of unidirectional CFRP. *Int J Adv Manuf Technol*:1–11 (2015).
20. Singh I, Bhatnagar N. Drilling of uni-directional glass fiber reinforced plastic (UD-GFRP) composite laminates. *Int J Adv Manuf Technol* 27(9-10) (2006), pp. 870–876.
21. Takeyama, H and N. Iijima. Machinability of glassfiber reinforced plastics and application of ultrasonic machining. *CIRP Annals-Manufacturing Technology*, 37(1) (1988), pp. 93-96.

22. D.H. Wang, M. Ramulu, D. Arola. Orthogonal Cutting Mechanisms in Graphite/Epoxy, Part II: Unidirectional Laminate Int. J. Machine Tools & Manuf., 35 (12) (1995), pp. 1639-1648
23. N. Bhatnagar, N. Ramakrishnan, N.K. Naik, R. Komanduri. On the machining of fiber reinforced plastic (FRP) composite laminates Int J Mach Tools Manuf, 35 (1995), pp. 701-716
24. Cheng H, Zhang KF, Wang N, Luo B, Meng QX. A novel six-state cutting force model for drilling-countersinking machining process of CFRP-al stacks. Int J Adv Manuf Technol 89(5–8), (2017), pp. 2063–2076.
25. H.A. Kishawy, S. Kanna, M. Balazinski. An energy based analytical force model for orthogonal cutting of metal matrix composites. Annals of the CIRP 53 (2004), pp. 91-94.
26. A. Pramanik, L.C. Zhang, J.A. Arsecularatne. Prediction of cutting forces in machining of metal matrix composites. International Journal of Machine Tools and Manufacture, 46 (2006), pp. 1795-1803.
27. D.M. Guo, Q. Wen, H. Gao, Y.J. Bao. Prediction of the cutting forces generated in the drilling of carbon-fibre-reinforced plastic composites using a twist drill Proc Inst Mech Eng Part B: J Eng Manuf, 226 (1) (2011), pp. 28-42.
28. Rao, G. V. G., Mahajan, P., and Bhatnagar, N. Three-Dimensional Macro-Mechanical Finite Element Model for Machining of Unidirectional-Fiber Reinforced Polymer Composites. Mater. Sci. Eng. A-Struct., 498(1–2) (2008), pp. 142–149.
29. L.M.P. Durao, M.F.S.F. de Moura, A.T. Marques. Numerical simulation of the drilling process on carbon/epoxy composite laminates Composites: Part A, 37 (2006), pp. 1325-1333.
30. W. Chen. Some experimental investigations in the drilling of carbon fiber-reinforced plastic (CFRP) composite laminates. International Journal of Machine Tools & Manufacture, 37 (1997), pp. 1097-1108.
31. Cheng, H., Li, Y., Zhang, K. F., & Luo, B. An efficient model for trust force dynamic analysis in drilling of CFRP/AL Stack. In Applied Mechanics and Materials Vol. 249 (2013), pp. 263-269.

32. Giasin, K.; Ayvar-Soberanis, S.; French, T.; Phadnis, V. 3d finite element modelling of cutting forces in drilling fibre metal laminates and experimental hole quality analysis. *Appl. Compos. Mater.* 2016.
33. Isbilir O, Ghassemieh E. Finite element analysis of drilling of titanium alloy. In: 11th International Conference on the Mechanical Behavior of Materials 10 (2011), pp. 1877–1882.
34. R. Zitoune, V. Krishnaraj, F. Collombet. Study of drilling of composite material and aluminum stack. *Compos Struct*, 92 (2010), pp. 1246-1255.
35. I.S. Shyha, S.L. Soo, D.K. Aspinwall, S. Bradley, S. Dawson, C.J. Pretorius. Drilling of titanium/CFRP/aluminium stacks. *Key Eng Mater*, 447-448 (2010), pp. 624-633.
36. E. Brinksmeier, R. Janssen. Drilling of multi-layer composite materials consisting of carbon fiber reinforced plastics (CFRP), titanium and aluminum alloys. *CIRP Annals – Manuf Technol*, 51 (2002), pp. 87-90.
37. Qi Z, Zhang K, Cheng H, Liu S. Numerical simulation for delamination during drilling of CFRP/al stacks. *Mater Res Innova* 19(sup6):S6): 98–S6):101 (2015).
38. S.A. Ashrafi, S. Sharif, A.A. Farid, M.Y. Yahya. Performance evaluation of carbide tools in drilling CFRP-Al stacks. *J Compos Mater*(2013), pp.1-14
39. R. Zitoune, V. Krishnaraj, F. Collombet, S. Le Roux. Experimental and numerical analysis on drilling of carbon fibre reinforced plastic and aluminium stacks. *Compos Struct*, 146 (2016), pp. 148-158.
40. Langella, A., Nele, L., & Maio, A. A torque and thrust prediction model for drilling of composite materials. *Composites Part A: Applied Science and Manufacturing*, 36(1) (2005), pp. 83-93.
41. Zhang, L. C., Zhang, H. J., & Wang, X. M. A force prediction model for cutting unidirectional fibre-reinforced plastics. *Machining Science and Technology*, 5:3 (2001), pp. 293-305.
42. D. Umbrello, R. M'Saoubi, J.C. Outeiro. The Influence of Johnson–Cook Material Constants on Finite Element Simulation of Machining of AISI 316L Steel *International Journal of Machine Tools & Manufacture*, 47 (3–4) (2007), pp. 462-470.

43. Zhang Y, Outeiro JC, Mabrouki T. On the selection of Johnson-Cook constitutive model parameters for Ti-6Al-4V using three types of numerical models of orthogonal cutting. 15th CIRP Conference on Modelling of Machining Operations 31(2015), pp. 112-117.
44. Jinyang Xu. Numerical and experimental study of machining titanium-composite stacks. Mechanics of materials physics.class-ph. Ecole nationale supérieure d'arts et métiers – ENSAM (2016).
45. HILLERBORG A., MODÉER M., PETERSSON P. E. Analysis of crack formation and crack growth in concrete by means of fracture mechanics and finite elements, Cement and Concrete Research, Vol. 6 (1976), pp. 773–782.
46. I Lapczyk, J.A. Hurta. Progressive damage modeling in fiber-reinforced materials Compos Part A, 38 (2007), pp. 2333-2341
47. Hashin Z., Rotem A. A cumulative damage theory of fatigue failure Materials Science and Engineering, 34 (2) (1978), pp. 147-160.
48. A Puck, H Schürmann. Failure analysis of FRP laminates by means of physically based phenomenological models. Compos Sci Techno, V58 (1998), pp. 1045-1068.
49. Puck A, Schürmann A. Failure analysis of FRP laminates by means of physically based phenomenological models—part B. Compos Sci Technol 62 (2002), pp.1633–62.
50. Vaibhav A. Phadnis, Farrukh Makhdum, Anish Roy, Vadim V. Silberschmidt. Drilling in carbon/epoxy composites: experimental investigations and finite element implementation. Composites: Part A, 47(2013), pp. 41–51.
51. Vaibhav A. Phadnis, Farrukh Makhdum, Anish Roy, Vadim V. Silberschmidt. Drilling in carbon/epoxy composites: Experimental investigations and finite element implementation. Composites: Part A, 47(2013), pp. 41-51.
52. I. Lapczyk, J.A. Hurtado. Progressive damage modelling in fiber-reinforced materials Composites Part A, 38 (2007), pp. 2333-234

53. A.S. Jahromi, B. Bahr, K.K. Krishnan An analytical method for predicting damage zone in orthogonal machining of unidirectional composites J Compos Mater, 48 (27) (2014), pp. 3355-3365

ACKNOWLEDGEMENTS

It took a lot of trial and error to complete my thesis. I would never have been to finish my thesis without the sincerely help and support from many people.

Firstly, I would like to grateful to Prof. Hyung Wook Park for giving me lots of advice and help to graduate study of mechanical engineering in Ulsan National Institute of Science and Technology. His advice and guidance allowed me to finish my research successfully. Also, I am truly gratitude to committee members Prof. Young-Bin Park and Prof. Namhun Kim. There were a lot of improvements because of their advice on manuscripts.

Also, I am really appreciate to Multiscale-Hybrid-Manufacturing Laboratory members for truthful advice and counsel of Dr. Deka, Dr. Hazarika, Dr. Sankara, Dr. Dong Min Kim, Anand P Jaiswal, Jisu Kim, Jaewoo Seo, Do Young Kim, Young Bin Kim, Woo Jin Lee, Min Ji Kim, Dongchan Kim and Oh Seop Kwon for their support.

Especially, Jaewoo Seo as senior researcher in Carbon Fiber Reinforced Plastic manufacturing helped me to complete my thesis. It was very happy to work with him in the same field. And thanks again to Dr. Dong Min Kim for giving me lots of ideas and knowledge in CFRP manufacturing field.

I would like to grateful to Gangwook Kwon, Jaehun Cha, Jinsik Kim and Jung-II Young a Makelab mebers who helped me with my experiments. They have helped numerous experiments and have been a great help in completing my thesis.

Finally, I sincerely thank to my parents for their considerable support and encouragement in completing my master degree.

